Muon Ionisation Cooling Experiment

MICE Note ???
IC-Pre/10-??
RAL-TR-???
Sheffield-Pre/10-??

July 17, 2012

The design, construction and performance of the MICE target

Abstract

The pion-production target that serves the MICE Muon Beam consists of a titanium cylinder that is dipped into the halo of the ISIS proton beam. The design and construction of the MICE target system are described along with the quality-assurance procedures, electromagnetic drive and control systems, the readout electronics, and the data-acquisition system. The performance of the target is presented together with the particle rates delivered to the MICE Muon Beam. Finally, the beam loss in ISIS generated by the operation of the MICE target is evaluated as a function of the particle rate, and the operating parameters of the MICE target are derived.

G. Barber, K.R. Long
Department of Physics, Blackett Laboratory, Imperial College London, Exhibition Road, London SW7 2AZ, UK

D. Adams, E. Capocci, E. McCarron, J. Tarrant,
STFC Rutherford Appleton Laboratory, Chilton, Didcot, Oxfordshire, OX11 0QX, UK

C.N. Booth, P. Hodgson, L. Howlett, R. Nicholson, E. Overton, P.J. Smith
Department of Physics and Astronomy, University of Sheffield, Sheffield, UK

Contents

1 Introduction

Muon storage rings have been proposed for use as sources of intense high-energy neutrino beams in a Neutrino Factory [1] and as the basis for multi-TeV lepton-antilepton colliding-beam facilities [2]. To optimise the performance of such facilities requires the phase-space compression (cooling) of the muon beam prior to acceleration and storage. The short muon-lifetime makes it impossible to employ traditional techniques to cool the beam while maintaining the muon-beam intensity. Ionisation cooling, a process in which the muon beam is passed through a series of liquid-hydrogen absorbers interspersed with accelerating RF cavities, is the technique proposed to cool the beam. The international Muon Ionisation Cooling Experiment (MICE) will provide an engineering demonstration of the ionisation-cooling technique and will allow the factors affecting the performance of ionisation-cooling channels to be investigated in detail [3]. Muon beams of momenta between 140 MeV/c and 240 MeV/c, with normalised emittances between 2 πmm and 10 πmm, will be provided by a purpose-built beam line on the 800 MeV proton synchrotron, ISIS [4], at the Rutherford Appleton Laboratory [5].

MICE is a single-particle experiment in which the position and momentum of each muon is measured before it enters the MICE cooling channel and once again after it has left (see figure 1) [6]. The MICE cooling channel, which is based on one lattice cell of the cooling channel described in [7], comprises three 20 l volumes of liquid hydrogen and two sets of four 201 MHz accelerating cavities. Beam transport is achieved by means of a series of superconducting solenoids. A particle-identification (PID) system (scintillator time-of-flight hodoscopes TOF0 and TOF1 and threshold Cherenkov counters CKOVa and CKOVb) upstream of the cooling channel allows a pure muon beam to be selected. Downstream of the cooling channel, a final hodoscope (TOF2) and a calorimeter system allow muon decays to be identified. The calorimeter is composed of a KLOE-like lead-scintillator section (KL) followed by a fully active scintillator detector (the electron-muon ranger, EMR) in which the muons are brought to rest. For a full description of the experiment see [6].

A schematic diagram of the MICE Muon Beam is shown in figure 2 [8]. A cylindrical target is dipped into the edge of the circulating proton beam. The depth at which the target is dipped into the proton beam is characterised by the 'beam centre distance' (BCD) which is defined to be the distance from the tip of the target to the proton-beam axis at the target's maximum excursion into the beam. Pions produced in the target are captured by a quadrupole triplet and transported to a dipole magnet by which the pion momentum is selected. A 5 T superconducting 'decay' solenoid follows the dipole. The additional pion path-length in the decay solenoid increases the muon-production efficiency. Following the solenoid, a second dipole is used to select the muon momentum and the beam is transported to MICE using a pair of large-aperture quadrupole triplets.

This paper is organised as follows. The requirements for the target system and an overview of its design are presented in section 2. Section 3 describes the design of the linear motor. The mechanical design of the target mechanism and the mechanical interface to the ISIS accelerator is presented in section 4. Section 5 describes the optical position-measurement system, the power

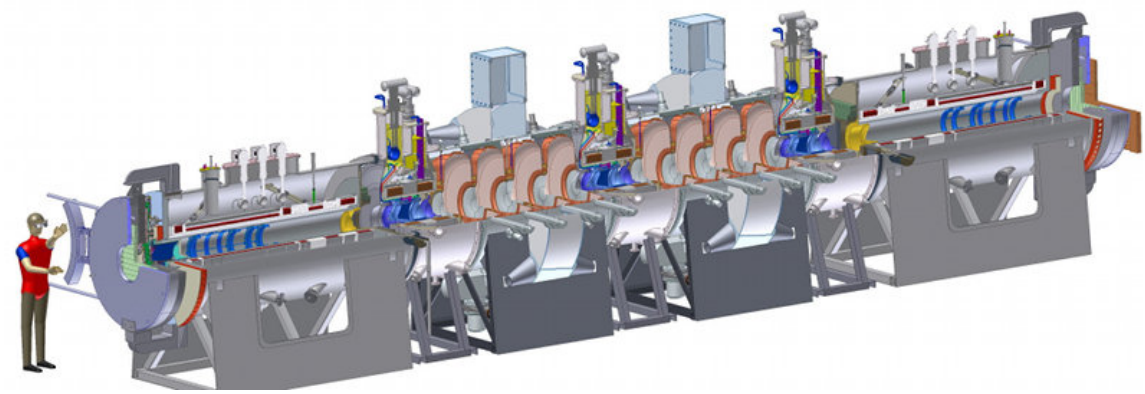

Figure 1: Cutaway 3D rendering of the international Muon Ionisation Cooling Experiment (MICE). The muon beam enters from the bottom left of the figure. The upstream PID instrumentation (not shown) is composed of two time-of-flight hodoscopes (TOF0 and TOF1) and two threshold Cherenkov counters (CKOVa and CKOVb). The upstream spectrometer is followed by the MICE cooling channel, which is composed of three 20 l volumes of liquid hydrogen and two sets of four 201 MHz accelerating cavities embedded in a solenoidal transport channel. This in turn is followed by the downstream spectrometer, a third time-of-flight hodoscope (TOF2), and a calorimeter system (KL and EMR).

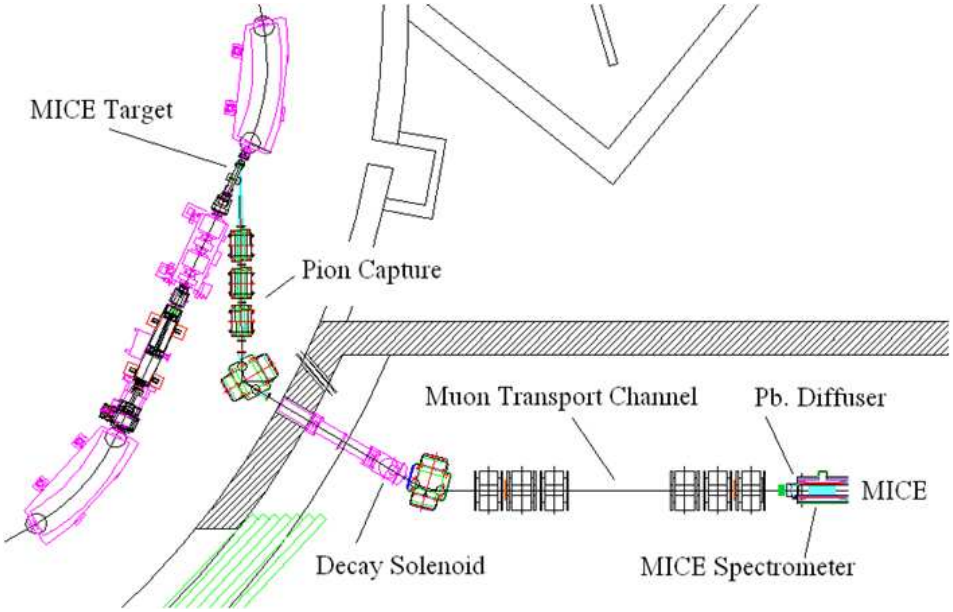

Figure 2: The MICE Muon beam-line

electronics used to drive the linear motor is described in section 6 and the control system in section 7. The performance of the system, the particle rate delivered for the MICE Muon Beam and the beam losses induced in ISIS are presented in section 8. Finally, a summary is presented in section 9.

2 Requirements and overview

The ISIS synchrotron [4] operates on a basic cycle of 50 Hz. Protons are injected with a kinetic energy of 70 MeV and accelerated to 800 MeV over a period of 10 ms prior to extraction. In the following 10 ms, the currents in the focusing and bending magnets are reduced to their initial values, ready for the next pulse of protons to be injected and accelerated.

MICE operation is parasitic to the functioning of ISIS and must cause minimal disruption to its principal function as a spallation neutron source. On selected pulses, the MICE target is caused to dip into the outer low-density halo of the proton beam just before extraction. Pions produced in the target emerge through a thin window in the ISIS vacuum system in the direction of the MICE muon beam line. On injection, the proton beam effectively fills the beam pipe. At the location of the MICE target, the beam has a vertical radius of ~ 67 mm. During acceleration, the beam shrinks to a radius of about 48 mm. To produce the required muon flux, the target must enter the beam by at least 5 mm, so a minimum travel of 24 mm is needed. (In practice, the exact position of the edge of the beam and the intensity of the halo show long-term variations. The position of the target at maximum insertion must therefore be controlled.) The target must be outside the beam envelope for the first 8 ms of the machine cycle, only entering the beam for the last 1 to 2 ms before extraction, when the protons are close to their maximum energy. The exact time of insertion must also be controllable.

In order to meet the demands described above, a linear electromagnetic drive was implemented to move the target vertically into the beam from above. The technical challenges are considerable. The mechanism must be extremely reliable, to avoid disrupting normal accelerator operation. It must provide an acceleration approaching $800\,\mathrm{ms}^{-2}$ in order that the target overtakes the shrinking beam envelope and is removed before the next injection. Operation must be precise and reproducible, both in position and timing relative to the beam cycle. The mechanism must operate within a high radiation environment, and all moving parts must use materials compatible with the stringent constraints of the accelerator's high-vacuum system. In case of any failure of the target mechanism, it must be possible to separate it both mechanically and in terms of vacuum from the synchrotron.

The complete target mechanism, described in detail in this paper, consists of a number of sub-assemblies.

- The linear electromagnetic drive assembly, which contains:
  - The shaft, forming the target at its lower end and carrying a set of fixed permanent

magnets, an optical readout vane at its upper end and a stop to prevent the magnets falling from inside the coils in the absence of power;

  - A pair of bearings to support, guide and align the shaft;
  - The stator, consisting of stationary coils with a water cooling system;
  - A central steel tube forming a vacuum barrier between the target shaft and the stationary coil unit;
  - An optical readout enclosure, with sapphire windows.

- The mechanical support assembly, which contains:
  - Flanges to provide accurate location of the stator and bearings;
  - Conflat seals, to ensure the integrity of the vacuum system.

- The mechanical and vacuum isolation system, to allow the unpowered target to be raised out of the beam, and the target vacuum to be separated from the accelerator vacuum. This contains:
  - A structural frame, carrying the weight of the target assembly;
  - A jacking unit and support structure with motorised screw-jack allowing a vertical travel of approximately 150 mm;
  - Centralising units and guide rods that guarantee the target returns to its predefined position when lowered into its operating position;
  - Edge-welded bellows, to allow relative movement of the components under vacuum;
  - A vacuum gate valve to isolate the vacuum systems.

3 Linear motor

A linear actuator was chosen as the most appropriate mechanism to drive the target into the beam. This implementation does not require any moving parts to cross the vacuum chamber walls, and can be realised without the need for lubricated bearings. For most of the duty cycle, the actuator is only required to exert a small force on the target, to keep it levitated out of the beam. At the appropriate time, a large accelerating force is required over a short period to accelerate the target into and out of the beam and then bring it to rest at its levitated holding position. For this short period, high currents can be employed.

The motor must be of a permanent magnet, brush-less design, as the high acceleration and large travel of the motor rule out the placing of coils on the moving parts. The integration of permanent magnets into the moving assembly removes the need for electrical contacts between the stator and the moving parts, simplifying the interface between the motor and the ISIS vacuum. The magnets on the moving components interact with the field produced by a set of stationary coils in the stator body. These coils are outside the ISIS vacuum, directly wired to

the driving electronics. Positioning outside the vacuum also allows the use of a water cooling circuit to remove the energy deposited by Joule heating of the coils.

The initial design of the linear motor was based on studies performed by an electrical engineer specialising in motor design, and outlined in [9]. The important constraints were to maximise the accelerating force while minimising the mass of the moving components. The mass of the magnetic materials thus form a significant fraction of the total mass. Different magnet and coil topologies were investigated, and the resulting design is documented in the following sections.

3.1 Electromagnetic design

Analysis of ISIS beam properties indicated that a peak acceleration of $950\,\mathrm{m\,s^{-2}}$ would give sufficient headroom for the target to achieve an appropriate interception with the beam given various beam conditions and a deep target actuation. The low mass of material required for interaction with the beam implies that the mass of the moving part of the motor (or "shuttle") must be dominated by that of the permanent magnet assembly and any mechanical linkages. A design was therefore required which maximised the electromagnetic force while minimising the mass, with the goal of a specific force equal to $\sim 950\,\mathrm{N\,kg^{-1}}$ for reasonable assumptions of motor geometry and location. To achieve the highest magnetic loading, sintered neodymium-iron-boron magnets were chosen for the shuttle, as these have the greatest field strength. A bank of appropriately energised coils interact with the field of the magnets to drive the shuttle. Soft magnetic core material was considered for the stator, but this was not found to lead to any advantage, due to the small size of the motor and the fact that magnetic material would be saturated [9]. This was exacerbated by the significant "air-gap" between the permanent magnets (inside the vacuum chamber) and coils (outside), actually filled by vacuum and non-magnetic vacuum tube.

Two magnetic topologies were considered for the shuttle, and compared using 2-D axisymmetric modelling. Multi-pole radially magnetised discs attached to a central soft magnetic core were found to provide a more efficient device than axially magnetised discs separated by pole pieces. The radial design is also less prone to demagnetisation [9]. The exact geometry was then improved by iterative finite element studies. Test results from a prototype motor were used to validate the design.

3.2 Stator

The stator, which is cylindrical in shape, contains 24 flat coils mounted around a thin walled steel tube. Individual coils, with an inner diameter of 18.3 mm, consist of 36 turns of copper wire and have an axial thickness of 2.85 mm. After winding, each coil is impregnated with insulating varnish to form a stable compact unit. During assembly six $25\,\mu$m copper shims are sandwiched between each pair of coils to facilitate heat conduction out of the coil stack. The addition of the copper shims gives a coil pitch of 3 mm. Connecting leads from the coils are led

radially outwards. Three thermocouples are inserted between three pairs of coils to enable the temperature of the coil stack to be monitored. A coiled copper tube soldered onto a solid copper jacket is placed around the coils and is in contact with the copper shims. This carries the cooling water, the temperature of which is monitored at either end with two more thermocouples. The entire assembly is inserted into an aluminium outer cylinder, the stator body, with the insulated copper wires and the cooling pipes emerging through a slit in the side. The individual coils are wired up at terminal blocks placed external to the stator body.

3.2.1 Coils

The stator contains twenty four identical coils that are stacked vertically and numbered one to twenty four starting from the top of the stator. The stator coils are responsible for interacting with the permanent magnets on the shaft both to levitate the target shaft when the target is being held out of the ISIS beam and to produce the accelerating force when the target needs to be inserted into the beam.

Each coil is composed of thirty six turns of 0.56 mm polyester-imide enamelled copper wire, over-coated with a polyamide-imide resin. This yields a high temperature winding wire that is rated to 200°C operation [10]. These coils are wound on an 18.1 mm diameter former, each coil having a depth of 2.85±0.1 mm. Coils outside this tolerance are rejected due to the limited space between coils and the required pitch of 3 mm. The clearance of ∼0.15 mm between the coils is used to insert thin copper shims which act as heat sinks. After winding, the outer diameter of the coils is 30 mm. Each coil is double dipped into a varnish that seals the windings and provides additional electrical insulation [11]. Each coil is tested to 1 kV before being built into a stator. A photograph of a finished coil and some of the inter-coil copper shims is shown in figure 3. The copper shims provide a thermal path between the coils and the cooling jacket. The inner diameter of the shims is 19 mm and the outer diameter 36 mm. The shims are split to reduce eddy-current losses.

3.2.2 Stator Bore

A thin walled non-magnetic stainless steel tube passing through the centre of the coils forms the stator bore. It provides isolation between the stator body and the ISIS vacuum and ensures the mechanical alignment of the coil stack. The nominal wall thickness of 0.5 mm is reduced to 0.3 mm where it passes through the coils. The reduction in magnetic field strength within the bore caused by the stainless steel tube was estimated to be 1%. The stainless steel tube is insulated from the coil stack using three layers of self-adhesive kapton tape.

3.2.3 Cooling Jacket

The cooling of the stator is extremely important as the rate of heat transfer from the coils to the cooling water ultimately limits the maximum rate at which the target mechanism can be

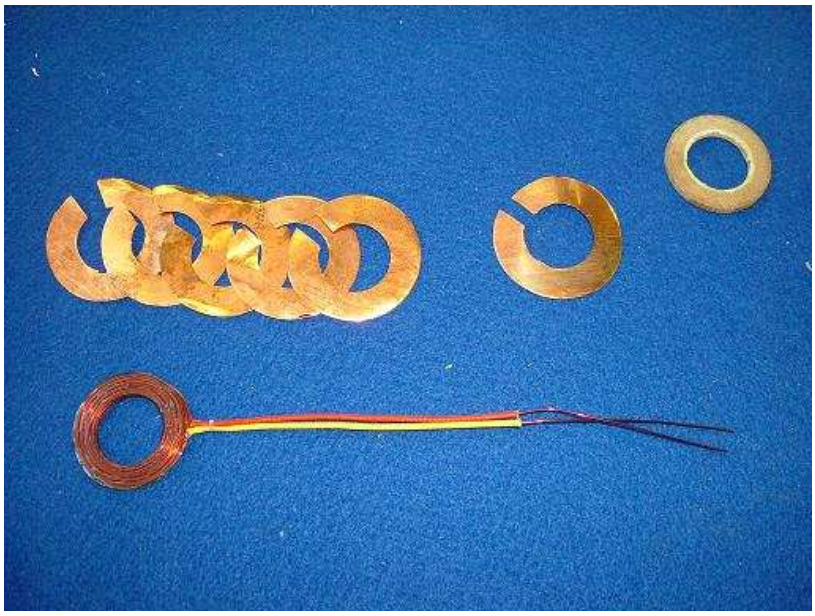

Figure 3: A complete stator coil and some copper heat-sinking shims.

actuated. Typically, when the stator is levitating the shaft out of the beam, the stator's power consumption is ∼30 W. Every time the target mechanism is actuated an additional heat load of 400 J is deposited in the stator coils. The coils are small and therefore the heat capacity of the coil stack is correspondingly low. Without any heat-sink the coils would rise in temperature by ∼ 5°C with every actuation. Therefore, if this heat is not removed quickly, repeated actuation of the stator will rapidly result in the temperature of the coils rising above their maximum rated working temperature of 200°C .

Unfortunately, the permanent magnets that are attached to the shaft will not operate up to this temperature without there being a serious risk of demagnetisation. The exact maximum safe operating temperature is hard to determine, as the Curie temperature is field dependent. There is also some evidence that the risk of demagnetisation at elevated temperatures is accentuated when running permanent magnets in a radioactive environment [12]. Running the stator for extended periods has demonstrated that coil temperatures of 80–90°C does not lead to demagnetisation.

A cooling circuit is required to remove heat from the coil stack. This consists of an external, water-cooled, split cylindrical copper jacket. The jacket has a thin-bore, copper cooling tube soldered onto its outer surface through which a flow of water can be maintained. This is illustrated in figure 4.

The inner diameter of the cooling jacket is slightly smaller than the outer diameter of the copper shims. When the jacket is slid over the coil stack this has the effect of bending the copper shims over, thus ensuring a good thermal contact between them and the jacket. A photograph of the jacket placed over the coil stack is shown in figure 5. The cooling pipe has a narrow bore and so the water flow rate is quite low. Typically, at ∼4 bar, a flow rate of ∼1 litre min^{-1} is achieved. This flow rate has proved to be sufficient to remove the heat from

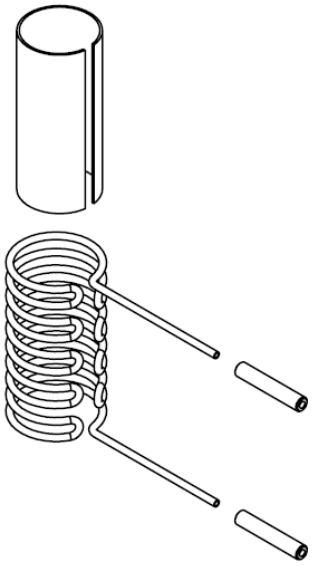

Figure 4: The copper cooling jacket is over-fitted with the water cooling pipes. The cooling pipes are soldered onto the jacket.

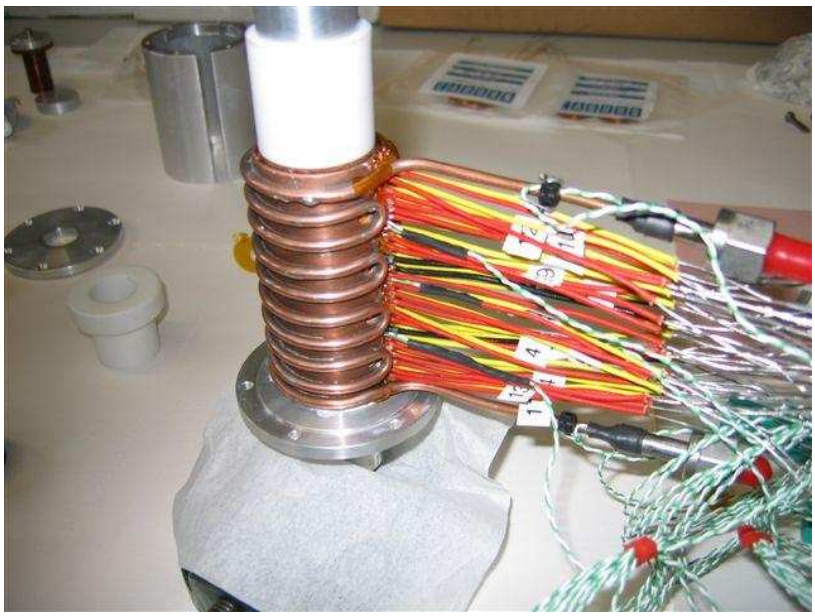

Figure 5: The cooling jacket, placed over the coil stack.

the coil stack during normal operation. A nominal stator operating temperature of 80°C has been maintained, well within the working temperature range of all the components.

3.2.4 Stator Assembly

The coil stack is assembled over a former that has the same diameter as the insulated bore tube. The stack starts with a spacer followed by four copper shims. A coil, lightly coated on both sides with a thermal paste to aid with heat-sinking, is added. Six copper shims follow. The second coil is then added to the coil stack and the process is repeated for all twenty-four coils. As each coil has a nominal thickness of 2.85 ± 0.1 mm the cumulative error is tracked and minimised during the coil stack construction by selection ofcoils of appropriate thickness. An assembled coil stack is shown in figure 6.

The split in the copper shims aids in keeping the coils parallel during construction. This is achieved by placing the split in the shim where the wires to the coil exit. (There is sometimes a small bump at this point on the coil due to the wire exiting from the centre of the coil back over the top of the other windings). The gap created by the split in the shims also allows thermocouples to be inserted into the coil stack.

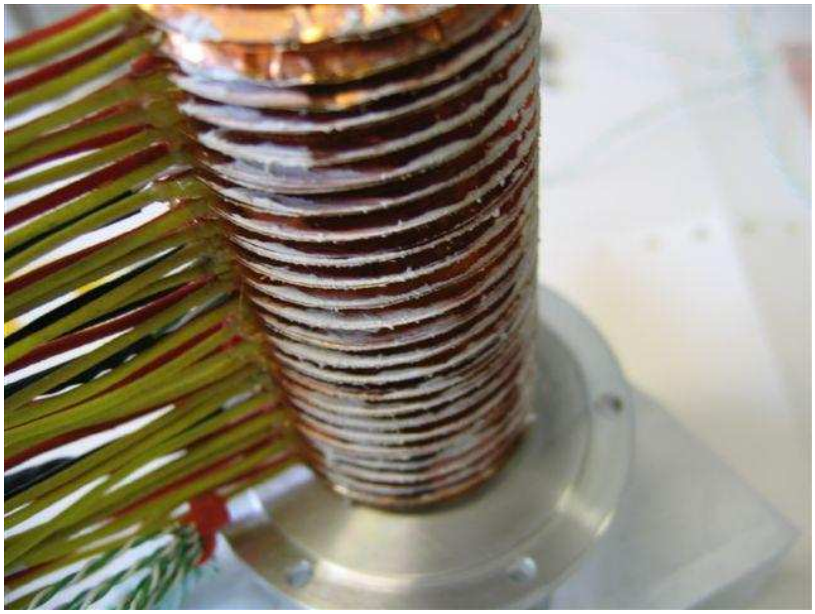

Figure 6: All 24 coils assembled on a former. The copper shims can be clearly seen protruding from the coil stack where they will later make contact with the cooling jacket.

At this stage a cooling jacket is slid over the coil stack. The stator body is then completed by adding a split outer jacket and two end-caps. The split in the outer jacket allows the wires and the cooling pipes to protrude for external connection. The end caps provide light compression on the coil stack, keeping it in place. The former on which the coil stack was formed is now removed and the bore tube inserted through the bore of the stator. A final electrical insulation check is then performed, to ensure that all coils remain isolated from metal parts including the bore tube and cooling jacket. The installation of the stator body into the core of the target drive assembly is described in section 4.

3.3 Permanent magnets

The permanent magnet assembly interacts with the field of the stator coils to produce the force on a central shaft which accelerates the target into and out of the proton beam. To achieve the maximum magnetic field, the assembly is constructed from sintered neodymium-iron-boron (NdFeB) magnets. Twenty-four segments are arranged in 3 rings, with 8 magnets per ring, as shown in figure 7. They are glued to a mild steel core to produce a cylinder that is 18 mm long with an outer diameter of 15 mm and an internal diameter of 4 mm. Thin ceramic washers separate the three rings. The central ring is 7.8 mm long, twice the length of the two outer rings. The whole assembly has a mass of about 25 g.

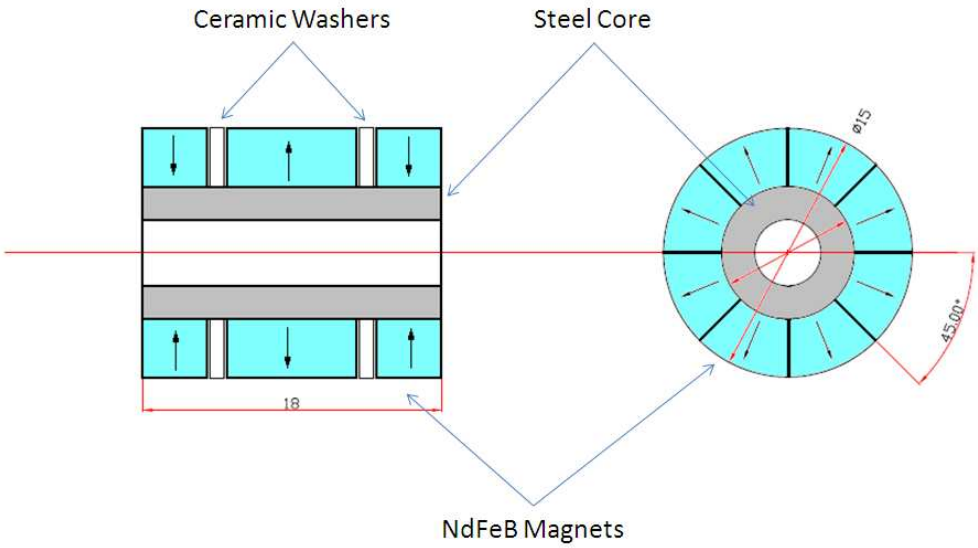

Figure 7: Drawing showing the structure of the magnet assembly

The individual sectors are manufactured by wire erosion from un-magnetised NdFeB material. The sectors are then magnetised radially and assembled in a jig before finally being glued in position using a strong two-component epoxy. Once the glue is cured, the magnet unit is lightly machined to the precise outer radius required. The middle ring is magnetised so that the outer surface is a North pole, while the outer rings have the opposite polarity. As a result of the relative polarisation of the rings, roughly circular flux lines are produced, as shown in figure 8. The peak radial component of the surface field of the magnets is approximately 0.6-0.9 T.

A FLUKA [14] simulation has been performed to ascertain the radiation levels expected around the target. Assuming 24 hour operation at 1 Hz for 180 days in a nominal year, the expected radiation dose to the magnets is estimated to be $\sim 1{\times}10^4$ Gy. To date, no evidence of degradation due to radiation has been observed.

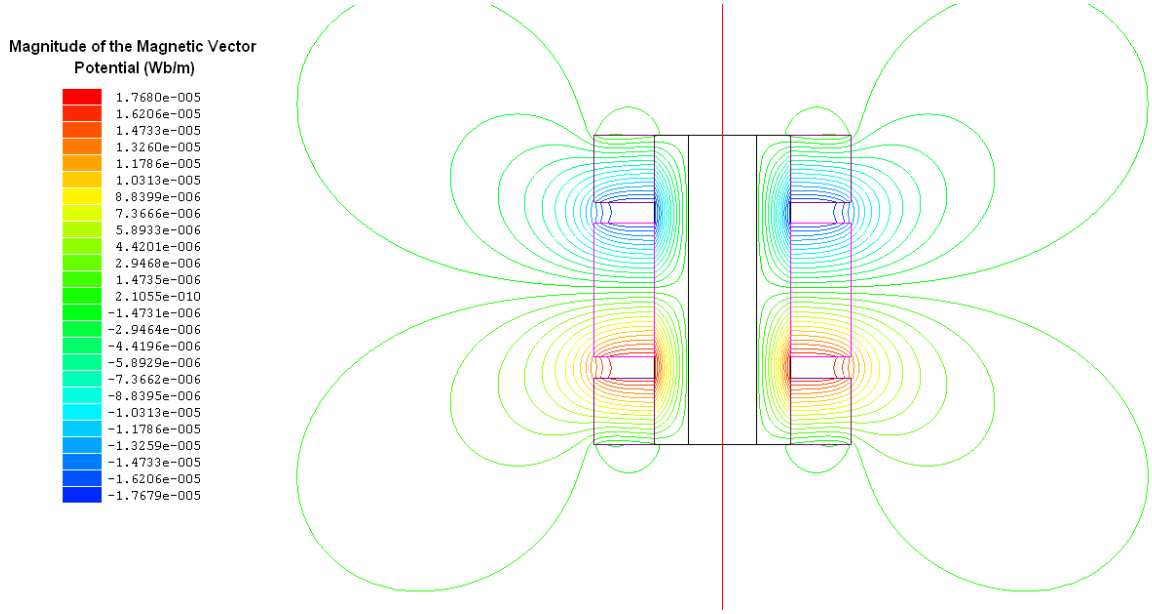

Figure 8: Diagram showing the flux lines from the permanent magnets as simulated by MAXWELL 2D Student Version [13].

4 Mechanical design and construction

The MICE target unit contains mechanical components and sub-assemblies that are designed to:

- Combine accurately all mechanical, electronic, electrical-power and optical-readout functions into a single unit;
- Provide a vacuum tight volume connected hermetically to the ISIS beam-line;
- Enable target operation by:
  - Providing controlled drive of the target's shaft into and out of the beam;
  - Enabling the velocity and location of the shaft to be determined;
  - Constraining the shaft along its path of travel thus preventing significant off-axis movement;
  - Providing stiffness in the shaft that resists significant deformation and vibration during operation.
- Eliminate the possibility of a failure that prevents continued operation of ISIS beam, including:
  - Breaking of the shaft such that part falls into the circulating beam;
  - Failure of welds or seals causing a leak into the ISIS vacuum chamber; and

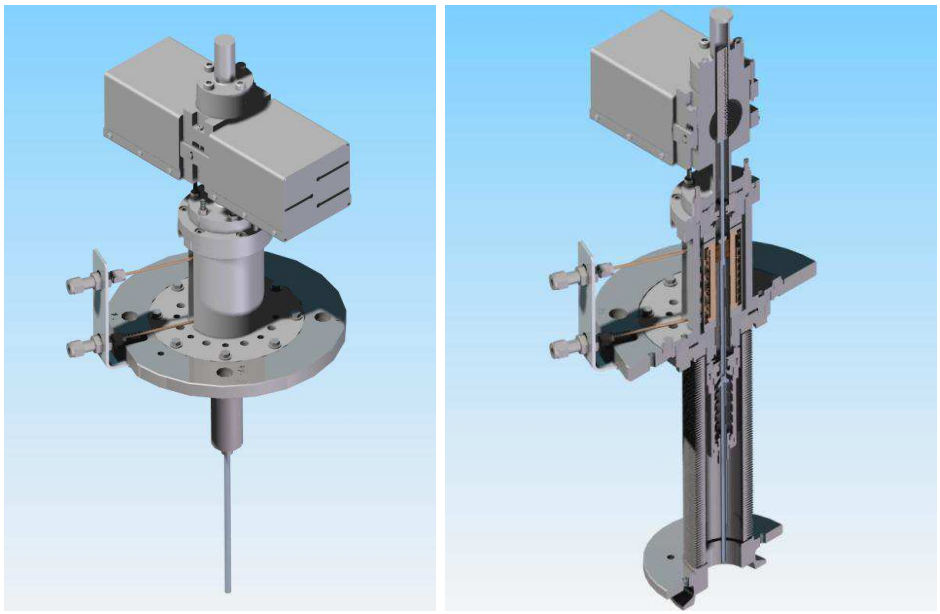

Figure 9: MICE target assembly, (left) with bellows removed, (right) a cutaway view (Descriptions and information on the components in the assemblies shown here follows.)

  - Contamination of the ISIS vacuum chamber, particularly with metallic or other dust that could contaminate the RF cavities.

- Deliver an operational lifetime that is sufficient to allow a rolling programme of maintenance at appropriately infrequent intervals.

4.1 Target shaft

The target shaft comprises of two sections of titanium (Ti) alloy grade 5 (6% Al, 4% V). The sections are a solid upper section and a lower tubular section with various functional features on each. The two halves are joined with a shrink-fitted plug-and-socket arrangement then electron-beam welded together. The shaft is coated with a hard diamond-like carbon (DLC) coating that acts as a bearing surface. The shaft is finally fitted with a permanent magnet, a slotted graticule for position read-out and the associated fixings and fasteners.

The shaft is 528 mm long and, when fully assembled with the magnet, slotted graticule and fixings, has a weight of $\sim$ 51 g. A radially segmented, permanent-magnet assembly is bonded to the shaft and held with a mechanical clamp. The stator accelerates and then decelerates the shaft in both the down-stroke and the up-stroke with a total travel in each direction of around 48 mm. The shaft achieves this 96 mm of reciprocating movement in about 30 ms before dwelling and then dipping again; with the dwell the shaft dips at a frequency of just under 1 Hz. The tip of the shaft has a cylindrical cross section of $\sim$11.5 mm^2 (5.95 mm outside diameter and 4.55 mm inside diameter); as it is an integral part of the tubular lower shaft it is grade 5 titanium alloy.

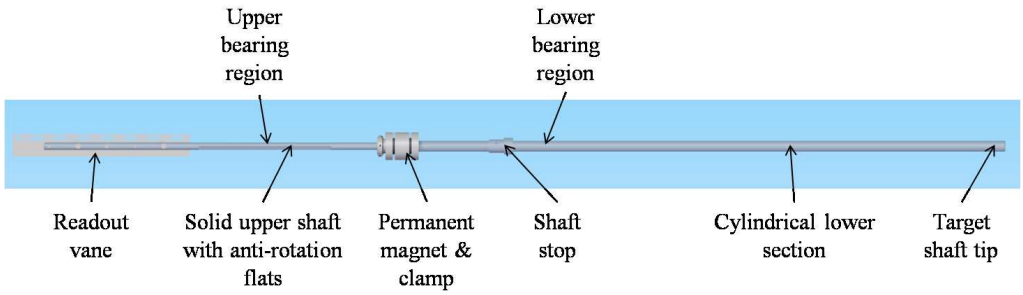

Figure 10: MICE target shaft assembly (shown horizontally oriented, operates vertically with tip down).

It is the tip of the hollow cylinder that momentarily grazes the halo of the ISIS beam to produce pions.

The production quality of the target shaft is the most critical aspect of all the manufacturing process. The shaft is manufactured within very tight dimensional and geometric form tolerances. The tight dimensional tolerances ensure the close fit of the shaft with the bearings; this tight fit accurately constrains the shaft's vertical motion. The shaft requires a high degree of straightness and good roundness. Tight tolerances of form (cylindricity and run-out) are applied to the manufacture of the shaft; accurate form minimises deformation and vibration of the shaft during the rapid acceleration and deceleration.

4.1.1 Design

Though form is accurately controlled, it is not perfect. Add to this a non-perfect constraint in the bearings and a stiffness limited by mass, geometry and material properties, then the rapid acceleration and deceleration of the shaft will cause it to deform and vibrate during operation. The stiffness of the shaft is very important. Increasing the stiffness of the shaft, without increasing mass, pushes up the frequencies of resonant modes. Increasing the frequencies, especially those of the first few resonant modes, reduces the number of resonant modes the shaft passes through as it is accelerated and decelerated. Excitation of vibrations in the shaft may arise from a number of sources, including:

- Large changes in velocity take place at ~ 15 ms intervals, i.e. twice over the 30 ms cycle. If the natural frequency of the shaft is close to 33 Hz or 67 Hz some distortion will be induced.
- The switching of power in the stator from one set of coils to the next may introduce an excitation force. The longitudinal driving force (up to 50 N) may be accompanied by off-axis torque or lateral forces as the sequential coil switching takes place during dipping. The frequency and severity of the excitation would be directly linked to the timing and magnitude of these forces. The timing of the switching is variable as the shaft is accelerated and decelerated in both directions, so the frequency of excitation is variable too. This may cause the shaft to pass through several excitation frequencies that correspond to the shaft's resonant frequencies. The magnitude of the excitation depends on the force seen by the

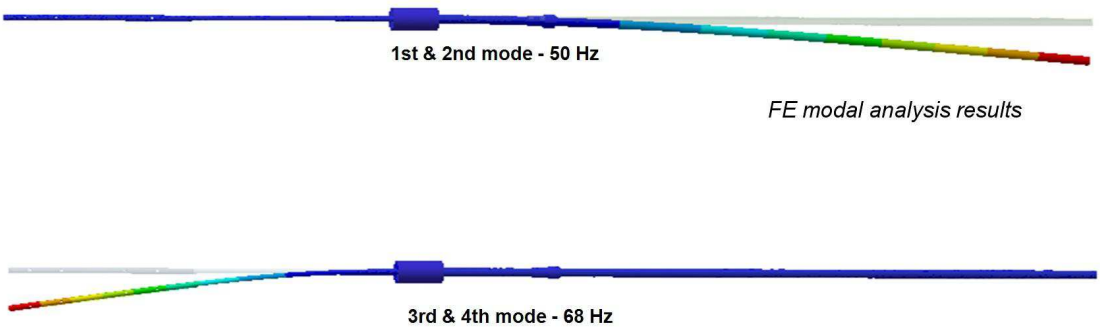

Figure 11: Output plot of FE modal analysis of shortened shaft with 'O' shaped lower section.

shaft when switching between coils; this is related to the quality of the coils and their axial location relative to the permanent magnet. With a 0.5 mm offset in coaxiality between the permanent magnet and the coil's magnetic centre the lateral forces have been calculated to be up to 2.5 N and the torque up to 32.5 mN m.

- The unit or surrounding support frames may be excited by the dipping shaft. There is potential for this vibration to transfer back from the support frame to the shaft through the stator and the bearings. There is significant vibration felt on the test frame after each dip.

A tubular, 'O' section shaft was shown to have sufficient stiffness. A finite-element (FE) modal analysis showed the 1st and 2nd resonant modes at 50 Hz, but the 3rd and 4th at 68 Hz.

The tubular lower section is created by rough-machining a bar to leave a slightly oversized external profile, including an integrated mechanical end stop. This is then heat treated to remove residual stresses. The bore is then wire eroded to 4.55 mm ID over the length of the lower shaft (about 320 mm); if internal stresses were present the shaft might deform along its length as this material is removed. After wire erosion the external profile, including the stop, is finished to final size referenced to the bore to maintain concentricity and thus material balance. Finally the socket for the shrink-fit joint is added.

The upper shaft stock material is stress relief heat treated before manufacture. It is then ground; this includes the flats which are very finely ground to ensure internal stresses are minimised. A larger diameter is left at one end onto which the socket for the shrink-fit joint is machined. Also added are the undercut for the magnet clamp and the fixing holes for the laser readout graticule. The very fine slot for the graticule is then cut by wire erosion. The wire erosion of this slot causes the two adjacent sections to open in a 'Y' shape. (This is only seen on the grade 5 titanium shafts and not on the previous versions made from commercially pure Ti grade 2; in fact the slot collapsed slightly when using Ti grade 2.) It appears the wire cutting is causing a slight expansion in the surface material on the inside of the slot that causes these sections to fan out. This has been resolved by supporting the shaft with the slot closed and stress-relieving back to a correct form.

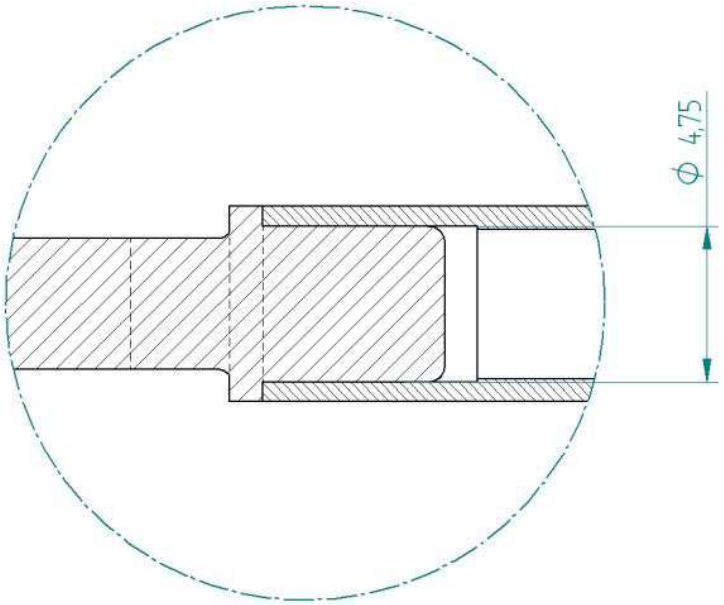

Figure 12: Plug and socket detail, upper shaft on left, lower shaft on right

To alleviate the risk of undertaking so many operations on a long single-piece shaft it is produced in two sections. The additional benefit of this is that they can be produced concurrently with benefits to the schedule. The lower shaft has an accurately machined socket and the upper shaft has a mating plug. The plug and socket are manufactured with a nominal 0.01 mm interference press fit. If these were pressed together at ambient temperature the material would cold weld. Cold welding is unlikely to be uniform and so the joint would skew causing a significant form error between the upper and lower shaft sections; it may even seize before it is fully pressed together. To achieve a clearance as they are assembled (i.e. to prevent cold welding or galling) the socket is expanded by heating to 250°C and the plug is shrunk by cooling to −190°C in nitrogen. A precision jig is then used to ensure correct alignment as the pieces are pushed together. The interference fit is made as the joint comes back to room temperature, contracting the socket and expanding the plug.

The two halves are further secured by welding at 8 points along the seam between the plug and socket using electron beam (EB) welding. A full circumferential weld was originally tried, however under-run or over-run at the end of the weld always made the two halves skew too much. Tensile testing was used to determine the strength of the shrink-fit and point-welded joint. Tensile testing broke the spot welds at 4 kN which coincided with an audible crack as the welds broke. After the welds broke the interference fit of the plug and socket prevented the shaft breaking into two halves; instead the tensile load began to climb in finite steps against displacement to 6 kN before the test was stopped. This was due to a cold welding effect; this is beneficial as it significantly reduces the chances of the shaft breaking into two should high impact load occur during a fault.

Figure 13: Failed weld and displacement of shaft halves after tensile testing

4.1.2 Material

Titanium is a good target material with respect to particle production, it is widely available, it can be easily worked and can be joined by welding. The shaft needed to be low mass to enable rapid and efficient acceleration by the stator. The shaft also needed to be stiff to minimise elastic deformation and vibration during its operation; titanium and its alloys have a good stiffness to mass ratio.

The initial redesign of the lower shaft led to the use of a tube with a mechanical stop welded on; tube in unalloyed grade 2 is widely available and was initially chosen for the shaft material. Impact testing was undertaken on this welded stop design; this closely represented a shaft's mechanical end stop impacting the lower bearing at a maximum speed of $9.3\,\mathrm{m\,s^{-1}}$ during a fault condition, including a safety factor of 1.5 A mass was dropped from a set height onto the stop on the lower shaft. This stop failed at around 4 impacts. In addition a bulge started to form in the wall of the tube due to the impact, see figure 14. Though the EB welding is a semi-automated process there is potential for variability in the strength of the weld, so the welded-on stop was not an entirely risk free choice. In addition the welding of the stop caused some distortion to the tube that had to be corrected by mechanical manipulation. It was decided to pursue a more costly manufacturing route to manufacture a stop integrated into the lower section from a single bar, a much stronger design. This overcame the restriction of obtaining only grade 2 tube and allowed consideration of titanium alloys.

Grade 5 (Ti-6AL-4V) titanium alloy was eventually chosen. There is a slight improvement in stiffness with the grade 5 titanium alloy over the unalloyed grade 2 titanium, 114 GPa and 103 GPa respectively. The additional strength of the grade 5, 895 MPa minimum over the 395ḾPa minimum of grade 2, is of no significant benefit as the loads on the shaft are minimal during normal operation and the integrated stop design is much stronger. The biggest benefit of grade 5 over grade 2 is in the hardness - Rockwell C 36 and 21 respectively in an annealed state. The harder alloyed grade 5 is easier to grind, allowing better finishes and tighter tolerances to be achieved. This is particularly useful for the upper shaft where the diameters and flats are ground.

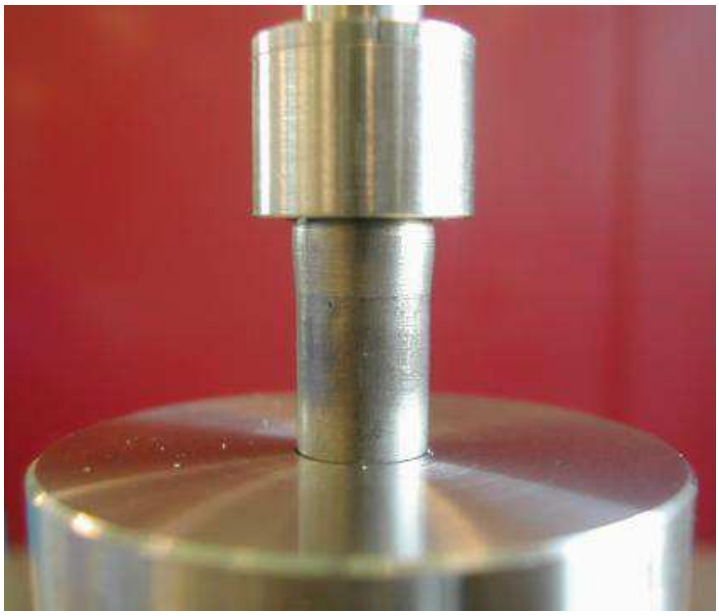

Figure 14: A bulge can be seen in the shaft under the stop. This occurred during impact testing.

4.1.3 Manufacture

Grinding is used to produce the main geometry of the upper shaft. The depth of cut in the grinding process is reduced towards the final cut to minimise the amount of deformation induced into the surface of the component; this in turn minimises internal stresses in the final shaft. Internal stresses may relax via strain over time leading to warping of the shaft. Grinding also gives the shaft a fine surface finish so that polishing removes only a minimal amount of material in achieving the final surface roughness of 0.05 Ra.

Stress relief annealing is undertaken on raw materials before processing as well as at certain stages throughout the processing. This removes internal stresses induced by manufacturing processes. Unrestrained heat treatment to around 670°C with a dwell period of $40 - 50$ minutes then a slow cool relaxes the stresses through strain, which deforms the material slightly. This deformation is removed during subsequent processing to achieve the final component's size with minimum internal stresses. The temperature and heat treatment cycle information was taken from [15].

A stress relief anneal is also applied to the assembled shaft prior to the final DLC coating process to straighten it. The shaft is held firmly and accurately in a jig, see figure 15. The jig is made from mild steel which is itself stress relieved (at 700°C) before an accurate 'V' is finely ground into it that supports the shaft. Mild steel has a similar coefficient of expansion to titanium alloy, 11 ppm/°C and 9 ppm/°C respectively; this means during expansion and contraction upon heating and cooling there will be minimal force induced by the jig on the shaft. Mild steel is also a dissimilar material to the titanium alloy so there is less chance of the jig and the shaft bonding at the elevated temperatures during heat treatment. The latest shafts have all undergone this process and have been straightened from >0.5 mm run-out post manufacture to around 0.1 mm

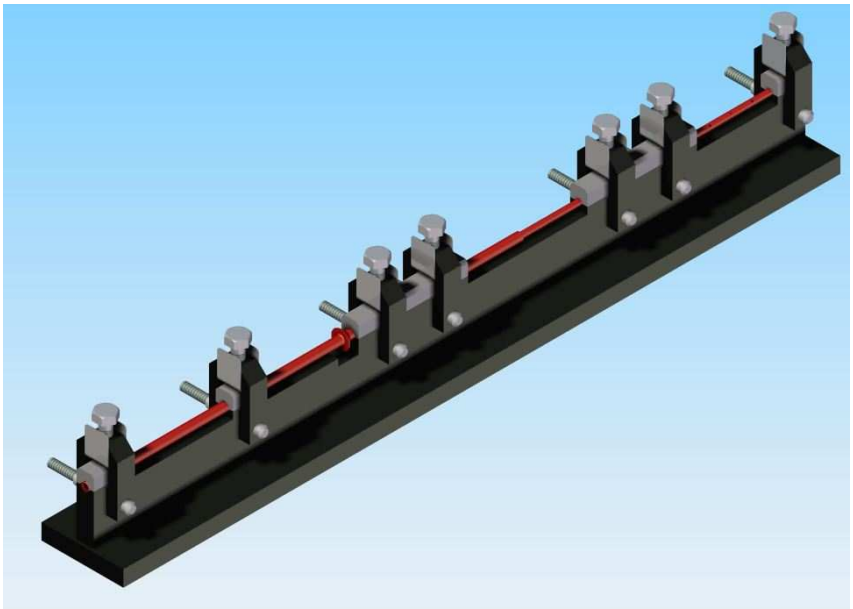

Figure 15: Shaft in straightening jig

run-out post treatment.

Conventional machining, such as milling and turning, is used on many features including the profile of the lower shaft, the fixing holes for the graticule and the plug and socket features used to join the upper and lower shaft sections.

Wire erosion is used to create a 90 mm by 0.22 mm slot in the upper shaft to support the graticule. The 4.55 mm inner diameter, 320 mm long bore through the lower shaft is also made by wire erosion.

The sub-components of the shaft, and the fully-assembled shaft, are inspected at many stages during manufacture to determine if they meet the specification on the technical drawings. Further information on the inspection of the shaft can be found in section 4.6.

Diamond like carbon (DLC) coating is applied to the bearing surfaces of the target shaft. The bearing surfaces are polished prior to DLC coating to ensure the final finish is smooth. The tip of the shaft that dips into the beam is not coated. The tip is left uncoated to prevent any thermal heating, from contact with the ISIS beam, causing failure of the coating through high temperature (>400°C) or through thermal strain differentials.

4.2 Target bearings

4.2.1 Description

Plain bearings support and constrain bearing regions on the shaft. There are two bearings, one to restrain the upper section of shaft and one to restrain the lower section. They are required

Figure 16: DLC coated shaft, dark grey/black coating extending over and beyond the bearing regions of shaft.

to constrain the lateral motion of the shaft as it dips, as well as incorporating an anti-rotation feature to prevent significant rotation about the longitudinal axis of the shaft. The upper bearing has the anti-rotation component; it is finely adjustable via screws to ensure accurate location with respect to the anti-rotation flats on the upper shaft. The bearings have plastic (Vespel® SCP5000) inserts and anti-rotation components (the dark items in figure 17). The plastic parts are assembled into stainless steel (Nitronic® 60) carriers. Nitronic® was chosen as it minimises cold welding when the fine location taper on the outside of the bearing carriers are lightly pressed into the tapered bearing seat in the 1.4404 / 316L stainless steel body.

4.2.2 Material

For the bearings the material and coating combinations at the bearing interface with the shaft were very important for function and longevity. A number of material and coating combinations have been trialled for use on the target. From the early trials of different coatings, a diamond-like carbon (DLC) coating on both the shaft and the bearing was found to be suitable. Despite these early successes, there subsequently appeared to be too much variability in the quality of this coating. This may have been due to the geometry of the parts being coated; the small bearing hole, even if produced in several segments, produced a "hollow cathode effect" in the RF coating chamber, thus variability in the thickness and adhesion of the DLC coating. This variability led to coatings on some shafts and bearings wearing away easily in later trials.

The alternative to DLC came from cryocooler technology as designed and built by STFC's Cryogenics and Magnetics Group. The cryocoolers have demonstrated in excess of 10^{10} cycles in a dry helium atmosphere. The material combination used in these cryocoolers is titanium (both commercially pure and 6% Al, 4% V) against Vespel® SP-3 grade. The SP-3 grade of Vespel® is

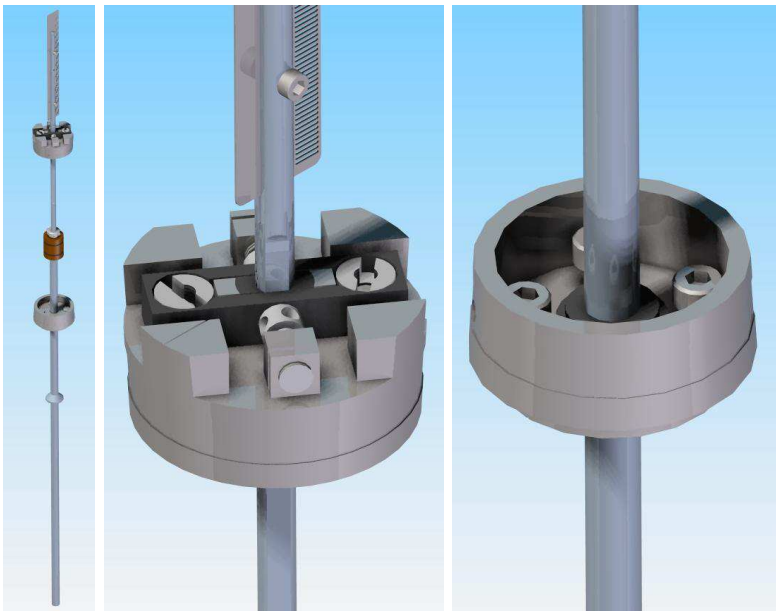

Figure 17: (left) Shaft and bearings, (middle) Upper bearing with anti-rotation, (right) Lower bearing

a polyimide that contains molybdenum-disulphide (MoS_2). MoS_2 is a dry lubricant which lowers the coefficient of friction. However MoS_2 was rejected on the grounds that long-lived isotopes might be produced in the high radiation environment. DuPont^{TM} Technical were contacted to determine if an unfilled alternative may be suitable. From the following requirements it was determined that Vespel® SCP5000 would meet the needs of the target when operating on the ISIS beam-line.

Bearing surfaces have a higher coefficient of friction in the ISIS vacuum 10^{-7} mbar [16], i.e. without the presence of moisture or lubricating films. A high coefficient of friction between bearing surfaces will increase the power required to drive the shaft, it will cause accelerated wear of the bearing surfaces and it will raise the temperature at the bearing interface through frictional heating. SCP-5000 was recommended for use as it has a relatively low coefficient of friction, even in a vacuum environment, of 0.26 or better [17].

Bearing materials are required to be tolerant to the effects of the nuclear radiation generated in ISIS, i.e. their mechanical properties must not change significantly during the operational life of the unit. Vespel® is a polyimide which will tolerate a significant total accumulated ionising radiation dose before a loss in mechanical properties.

Particles created during wear should be kept to a minimum. If they are created they must be managed and contained within the unit. This is particularly important for particles that have become activated, for health and safety reasons. In addition particles should not be released from the unit as they may damage the RF cavities adjacent to the MICE target in ISIS. Dust is produced when using the Vespel® bearings, however with a finely polished shaft this has been minimised. The target unit has been fitted with an extended housing with dust traps to prevent the dust produced from the Vespel® escaping outside of the unit, see figure 18. The bearing

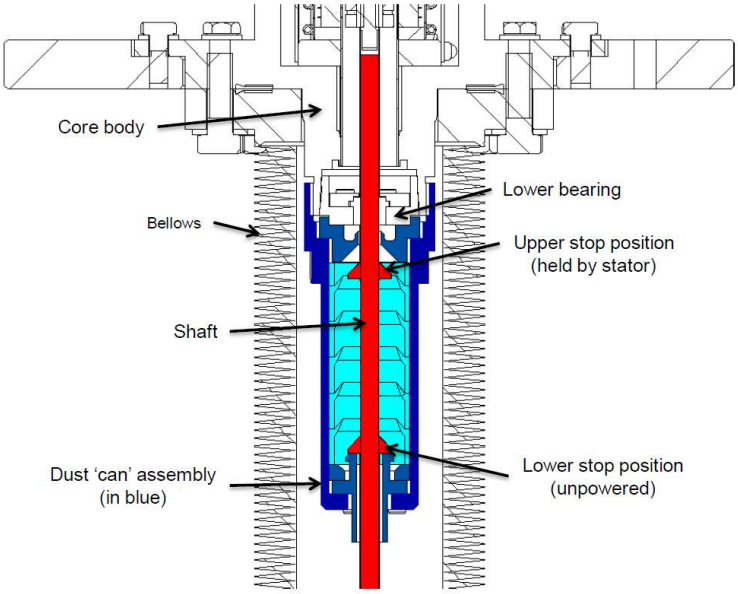

Figure 18: Dust 'can' assembly, that captures the dust below the lower bearing.

surfaces need to withstand a significant operational life and be able to be manufactured with fine surface finishes and tight tolerances to minimise the rate of wear; Vespel® is a relatively hard plastic so suits this.

The material must not significantly out-gas in the ISIS vacuum. Out-gassing tests were undertaken on vacuum baked samples of Vespel® SCP5000 (80°C for 72 hours) and were acceptable for use on the ISIS beam-line provided the total volume used was kept below 3 cm^3.

4.2.3 Rotational constraint

The upper section of the shaft has a pair of finely polished parallel flats that run against a flat faced Vespel® anti-rotation component on the bearing, see figure 19. The flat faces of the anti-rotation component are finely adjusted so that the flats on the upper shaft only contact them if the shaft rotates. In trials using an anti-rotation component with two completely flat faces, it was found that after running for some time the corners of the flats on the upper shaft would dig-in to the plastic and cause the shaft to temporarily lock; the semicircular reliefs shown in figure 19 were added to prevent this.

4.3 Stator

4.3.1 Description

The stator assembly surrounds the middle portion of the shaft assembly, including the permanent magnets which are driven by the stator. The bearings and stator assembly are fixed in the core

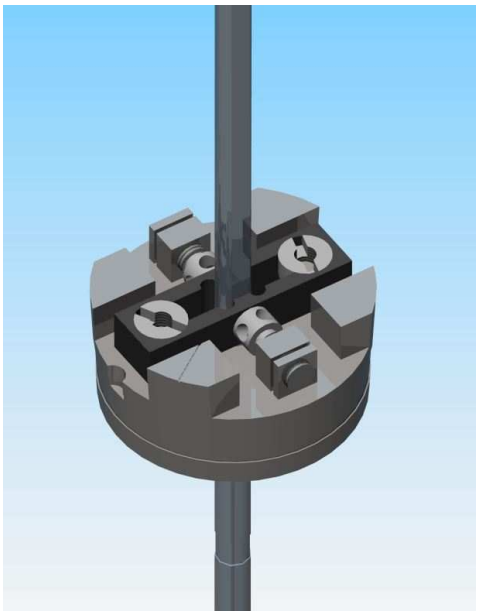

Figure 19: Upper bearing with Vespel® bearing insert and anti-rotation component

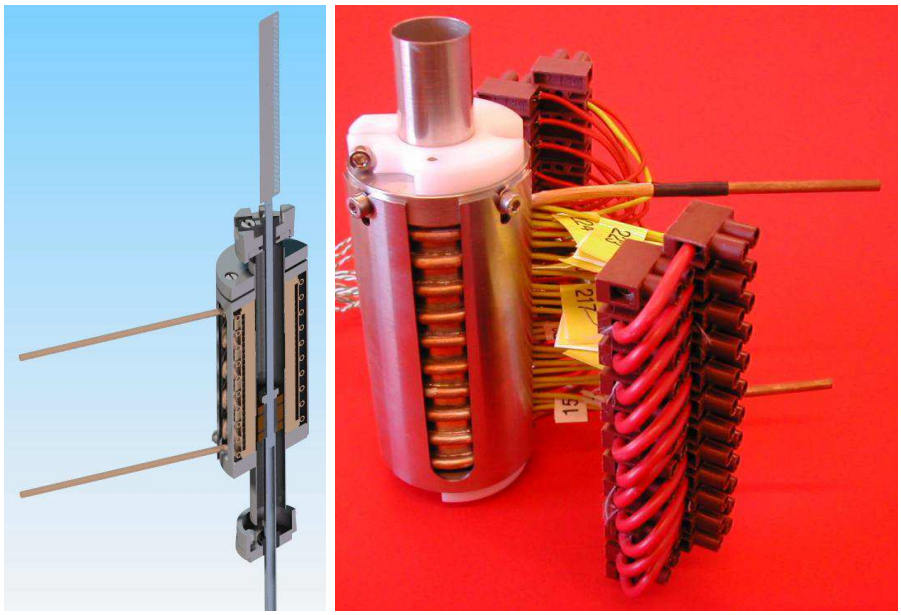

Figure 20: (left) Stator assembled with shaft and disc spring plate on top, wiring not shown; (right) Tested stator unit ready for assembly (shown with temporary plastic clamps).

structure (see below) to coaxially align the shaft assembly and permanent magnet with the stator coils.

The stator, described in section 3.2, is a self-contained sub-assembly; it is assembled around, but not fixed to, the central vacuum tube. As it is self-contained it can be tested independently. After assembly and test the stator unit is incorporated into the target unit by welding the ends of the vacuum tube into the two main core body components. The tube and welds provide an

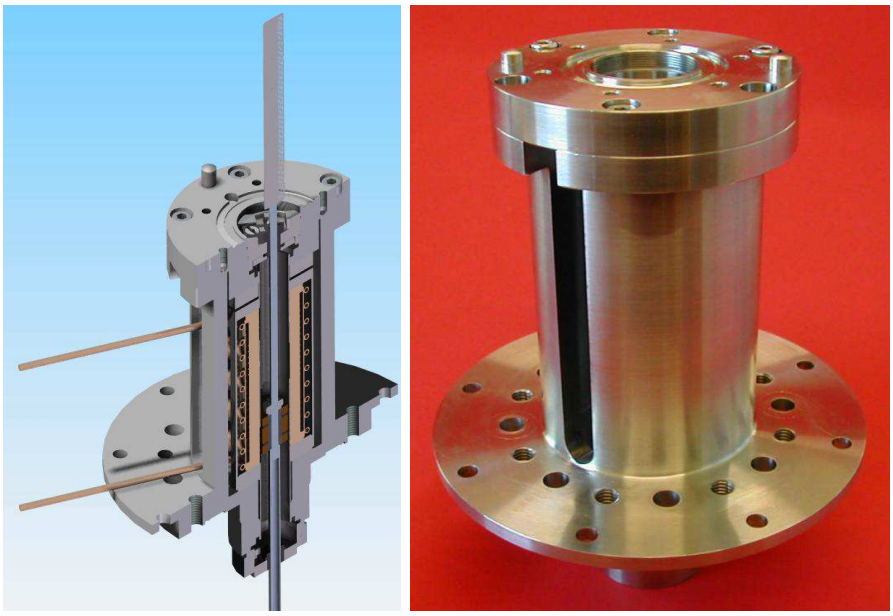

Figure 21: (left) Core body assembly with welded vacuum tube, (right) core tube body with upper flange assembled on top with fasteners and taper dowels.

uninterrupted vacuum volume though the middle of the unit. Above and below this central vacuum tube, the components are fixed to the body with copper knife edge (CF) seals. When the stator drives the shaft there is a reactive force of up to 50 N. As the stator is not fixed to the vacuum-tube this load is not transferred to the vacuum tube welds. To prevent the coils within the stator moving, or the stator moving as a whole, the stator unit is clamped down inside the core body using three stacks of disc springs. These springs exert a clamping force of around 100 N onto the stator unit when the upper flange of the core body is fully tightened onto the core tube.

4.4 Core structure

The core structure of the target is provided by two robust stainless steel (1.4404 / 316L) components, the core tube body and the upper flange. These contain the stator unit and the bearings. The other components of the target assembly, such as the electrical wiring and the covers, are also fastened to these core components.

The core is required to align the other components accurately and stably, in particular to provide the accurate coaxial alignment of the permanent magnets on the shaft and the stator coils. Careful consideration of the interfaces between the permanent magnet and the stator coils was required. The order of the interfaces relating to this critical alignment of the permanent magnet and stator coils are represented by '→', and are shown below:

Permanent magnet → Shaft → Bearings → Core structure → Vacuum tube → Stator coils.

This number of interfaces requires each component to be manufactured to tight tolerances,

then accurately assembled with respect to each other. Coaxial alignment between the permanent magnets and the magnetic field of the stator reduces or eliminates off-axis torque or lateral forces on the magnets as they pass through the stator's changing magnetic field.

Accurate alignment of the bearings is also very important. The bearing alignment, bearing-bore accuracy, straightness of the shaft and tolerances on the outer diameter of the shaft all build up to increase the minimum radial clearance tolerable between the bearings and the shaft. Keeping this radial clearance to a minimum ensures the shaft's travel is well constrained. If the radial clearances have no added compensation for manufacturing variations, the fit could be too tight which may lead to flexing of the shaft and possible fatigue failure or high power loading on the stator. To achieve accurate bearing alignment the core structure and the way it supports and locates the stator assembly has been simplified to the minimum number of components and interfaces. There are only two components and three interfaces between the 2 bearings:

Bearing → Core lower → Core upper → Bearing.

Minimising the components and the interfaces is a practical solution for machining as there are few tight tolerances to be achieved. To further aid the accuracy of alignment of the bearings and reduce the manufacturer's liability in achieving tight tolerances, the two core parts are made with a slight clearance fit, they are then assembled, inspected, adjusted to achieve a tight coaxial alignment, then dowelled together. The Taylor Hobson Talyrond is used to undertake the inspection of the alignment of the core body components. The bearing seats are aligned to each other within 20 μm of run-out; the repeatability of reassembly alignment with the taper dowels is around 10 μm.

The bobbin that supports the stator has a central bore where the permanent magnet runs up and down. The bobbin is welded into the core assembly so that it forms a hermetic seal from the flange on the upper flange to the flange on the core tube body. These flanges incorporate CF-type seal features which use knife edges to compress copper seals. A hermetically sealed internal vacuum volume is created when the optical housing and bellows are fitted to the core assembly and the bellows are then fitted to the vessel in the ISIS ring or the test vessel.

The core tube body has a small flange which is fitted with a larger flange extension. This extension is the main reference component for positioning the assembly on ISIS. Rods are suspended from a frame, either above the ISIS beam-line or on a test vessel in a separate building (for offline running and trials), as described in the next section. These rods fix to the larger flange extension and support the target unit for connection to the beam-line or vessel. Connection to the beam-line or vessel is made via a bellows component. The two-part flange is a practical solution for manufacturing as it minimises the material cut away from stock billets to form the components. The framework that the rods attach to is motorised. This enables the target unit to be lowered into position; the bellows compress when this happens. If there is a serious fault with the target unit, the motorised stage will drive the target unit up away from the ISIS beam-line past a shut off valve. This valve can then be closed to isolate the MICE target from the ISIS beam-line.

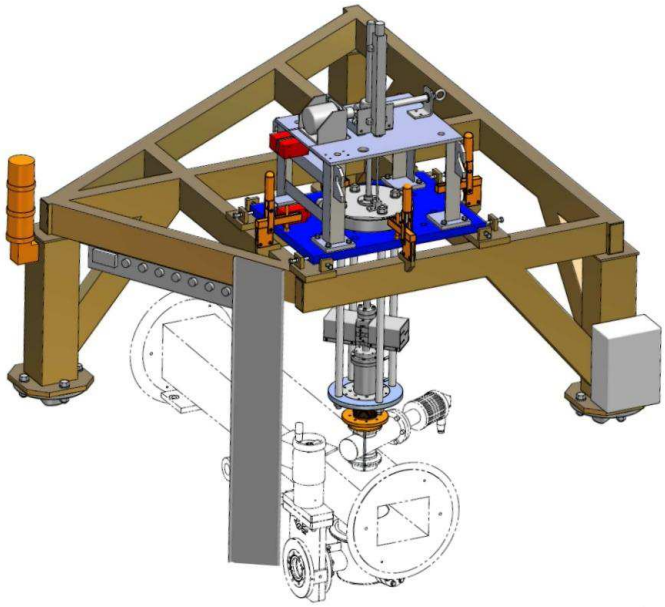

Figure 22: Target assembly suspended by rods from motorised stage above ISIS beam line, connected to beam-line with bellows.

4.5 Mechanical integration

The target mechanism must be rigidly supported in a manner which minimises the transfer of vibrations caused by the linear motor to the synchrotron itself. The target must also be removed from ISIS when it is not in use and complete isolation must be possible in the case of a fault developing in the mechanism. These objectives are met by suspending the target from a heavy, rigid steel frame which is itself bolted to pillars resting on the synchrotron floor, see figure 22. A motorised platform raises and lowers the target drive, which is connected to the beam-pipe via a set of extensible bellows and a remotely operable valve which can separate the vacuum systems of the synchrotron and the target drive. A duplicate section of beam-pipe, complete with target support frame, is situated in an assembly hall where all target mechanisms were commissioned.

4.5.1 Motorised platform

A heavy steel plate rests on the main support frame. This carries a motorised screw jack driven by a stepper motor (see figure 23). The jack can raise and lower a steel ring, which carries the main target mechanism via three sturdy rods passing through holes in the plate. The jack has a travel of 200 mm and, when in its lowest position, the ring fits into a locating socket. The motor is controlled remotely, and limit switches indicate when the mechanism is at its highest and lowest positions. The switches are interlocked to the control system to prevent the equipment from being driven outside safe limits. An independent position switch is linked to the Personnel Protection System, and prevents access to the MICE Hall when ISIS is operating and the target mechanism is lowered.

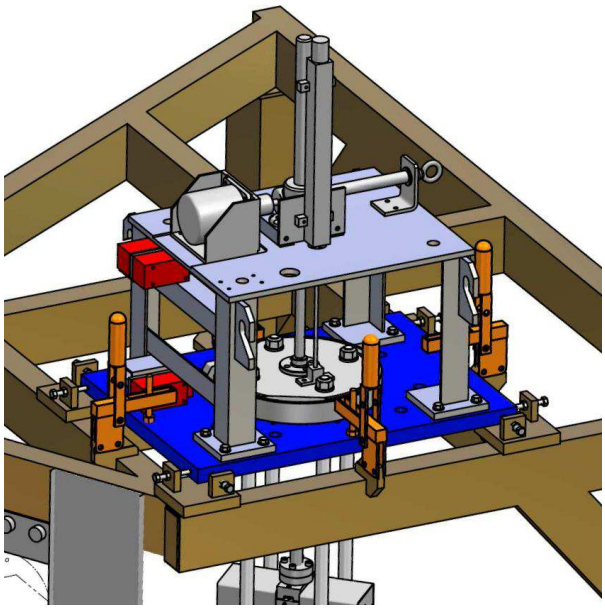

Figure 23: Motorised platform.

The plate is supported on levelling screws, and its lateral position is adjusted with locking screws to ensure the target is centred over the port in the beam-pipe. Once positioned, the plate is clamped in place.

During normal target operation, the support frame is moved to its lowest position. The tip of the target shaft is then outside the beam envelope only while it is magnetically levitated. When the target is not in use, the frame is raised to its highest position and the target is well clear of the beam even if powered down.

4.5.2 Bellows and ISIS vessel interface

To allow vertical movement of the target drive while maintaining a vacuum seal, the lower flange of the drive is connected to the beam-pipe using edge-welded bellows (see figure 24). These have an internal diameter of 46 mm, a compressed length of 56 mm between flanges and an extended length of 260 mm. The UHV seal between the bellows and target flange is maintained with a standard Conflat seal and copper gaskets.

As a fault in the target mechanism could compromise the ISIS vacuum, it is important that the target vacuum space can be isolated from the accelerator. This is achieved with a gate valve, mounted between the flange on the upper face of the vacuum vessel and that at the lower end of the bellows. Seals are formed using aluminium gaskets compressed by V-band clamps. The valve is operated by a low-pressure nitrogen line, controlled remotely, and has an aperture of 40 mm to allow the passage of the target shaft. The control system ensures that the target frame cannot be lowered while the valve is closed and that the valve cannot be closed unless the frame is at its upper limit switch.

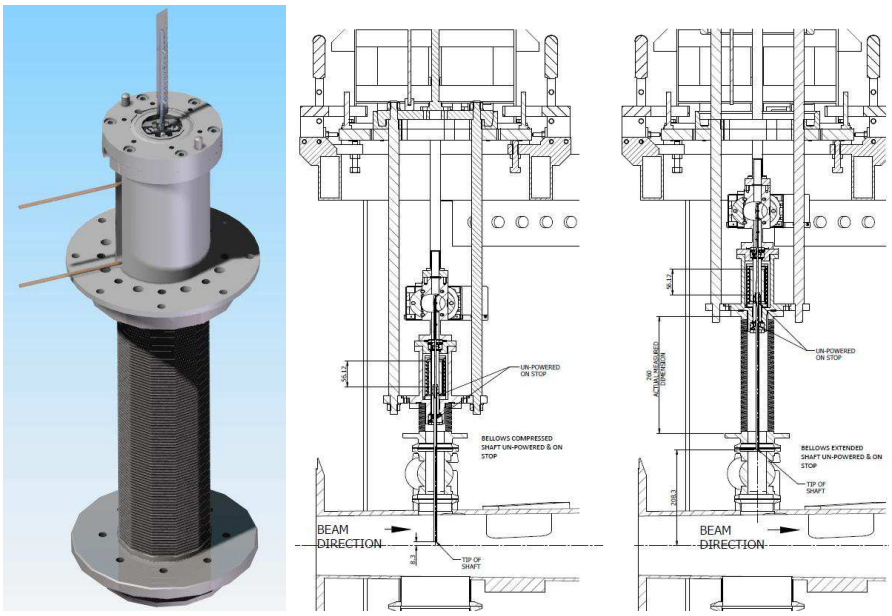

Figure 24: (left) Bellows shown assembled under core tube body; (right) Compressed and uncompressed bellows states.

The ISIS vessel is adapted for the presence of the MICE target in several ways. As well as the port on the upper surface to accept the target mechanism via the gate valve and bellows, it has a thin-walled steel window to allow the passage of pions, produced by interactions in the target, into the MICE beam-line. In addition, it has a glass inspection window directly below the target. This allows visual observation of the target.

4.6 Quality assurance and quality control

4.6.1 Shaft measurement

The shaft cannot be manufactured perfectly straight due to its long thin shape; however as long as the form is controlled within tolerable limits operation will be acceptable. During manufacture care is taken to produce the shaft sections with the best possible straightness thus minimising run-out between the bearing regions as well as finely balancing material about the axis of the shaft. Manufacturing includes the use of jigs to hold the shape during processing, heat treatment stages to relieve stresses and a final constrained heat treatment to achieve the desired shape. Shafts are accepted with a run-out between bearing regions of less than 0.12 mm; through prototyping it was proved that shafts with around 0.12 mm of run-out between bearing regions would operate acceptably in the target unit.

The size of the shaft is very easy to measure using conventional micrometers. The shape however is more difficult. For the shaft a Taylor Hobson Talleyrond is used to measure the run-out between the lower bearing region and the other parts of the shaft. The Talleyrond has a rotating table onto which annular parts are clamped; a probe on an extending arm then

Figure 25: Talleyrond with jig, jig being aligned vertically for shaft measurement using gauge rod.

measures the exterior of the annular component as the table rotates. A jig was produced for shaft measurement that allows the Talleyrond to access relevant sections of the shaft for measurement. It uses an upright post to support a collet assembly; by lightly press fitting the shaft into the collets then the collets into a holder the shaft is secured and aligned. The larger diameter lower bearing region is chosen to be the datum to which all other surfaces are measured. The Talleyrond is programmed to locate this surface by measuring the circumference over a number of positions along its axis. The Talleyrond then aligns the lower bearing region with the axis of rotation; it does this by automatically adjusting the plane of the table. Next it is programmed to measure the other sections of the shaft. Again the Talleyrond measures the circumference over a number of places along the axis of the region to produce a profile of slices. These 2-D slices can be stacked to produce an extrapolated 3-D model of the shaft as well as being referenced to the lower bearing datum. The probe has an extremely light touch (1.5 mN), however this is enough to elastically bend the shaft when measuring further away from the collet supports. A fine sprung-arm counter-balance is placed to oppose the probe arm to counteract any forces from the probe during measurements.

4.6.2 Magnetic inspection

To characterise the magnetic performance of the target mechanism, magnetic measurements are carried out on the stator and on the permanent magnet assembly. The equipment used is a three-axis Hall probe mounted on the end of a travelling arm. The position of the probe can be set to a resolution of 1 μm in three axes.

Stator

For the stator, measurements are required to define the position of the magnetic centre of the coils relative to the mechanical centre. If the coils are offset, the small radial field they generate may have the effect of moving the shaft laterally as it passes through the stator. Accurate alignment of the magnetic centre is therefore important to minimise wear on the bearings during operation.

The coils are powered using a constant current of 7 A; this is lower than the peak current when the shaft is dipped into the beam due to heating concerns - a constant current of 60 A would overheat the coils. A current of 7 A heats the stator to around 50°C when water cooling is used.

The stator is set up and aligned to the measurement bench. A cross-hair on the end of the Hall probe is viewed through a telescope as the probe is moved up and down the bench; this allows the telescope axis to be set parallel to the bench axis. Cylindrical inserts with a precisely machined central hole are placed in either end of the stator bore in turn, to allow the stator axis to be aligned parallel to the bench axis. The estimated accuracy of this procedure is around 100 μm at each end, which gives an overall alignment accuracy of 0.8 mrad over the 180 mm length of the stator.

An initial scan of the stator along the longitudinal (z) axis shows a series of peaks corresponding to the individual coils. To find the centre of each coil, a two-dimensional scan at each peak position is carried out. The magnetic centre is the point at which the longitudinal field is a minimum. The longitudinal field is fitted to the function:

$$B_z = ax^2 + bx + cy^2 + dy + exy + f$$

The centre point can then be found from the fit to the data.

Permanent magnets

For the permanent magnets, measurements are carried out to determine azimuthal variability of the radial field (i.e. B_r vs θ). Due to variations in the PM blocks, there is a certain amount of variation in the peak (and trough) values of the radial field. An assembly with smaller differences between the peaks would be preferable, as it may reduce lateral movement and vibration of the target shaft during operation.

The PM assembly is attached to a rotational stage in order to map the radial field as a function of angle and longitudinal position. In this case, the Hall probe is attached to a spring-loaded head to keep it the same distance from the PMs (about 1 mm) as the assembly is rotated. This was found to be necessary since the PM assembly was not parallel to the Hall probe axis. The effect is small - a few tens of microns as the PM assembly is rotated - but enough to give a significant difference in the measured field, as the field drops off rapidly with radius.

5 Optical position-measurement system

In order to switch the current through the stator coils at the correct time to drive the target shaft, it is necessary to sense the exact position of the shaft while it is moving. To avoid disrupting the motion of the low mass shaft by mechanical contact, and to remove the necessity for electrical feed-throughs traversing the vacuum wall, an optical method is adopted. Furthermore, since active electrical components would not survive in the high radiation environment near the target, optical fibres are used to convey the optical signals, with all sensitive electronics being placed outside the accelerator vault (in the experiment control room some 100 metres away).

A graticule or vane attached to the shaft and interrupting a light beam will generate a series of pulses, which could be used to determine the speed but not direction of movement of the shaft. If it is arranged that two beams are interrupted by the vane, with the pulse trains being 90° out of phase, then both speed and direction can be inferred. (Such quadrature encoders are used in many commercial movement detectors.) With a third beam producing a pulse at only one well-defined point, a zero of position can be defined. In this way, by counting pulses away from the zero, an absolute position measurement can be made.

In addition to providing feedback to the controller, position measurement allows the trajectory of the target to be monitored and recorded by the data acquisition system, allowing long-term reliability and stability to be monitored and fault conditions to be diagnosed.

5.1 Optical vane

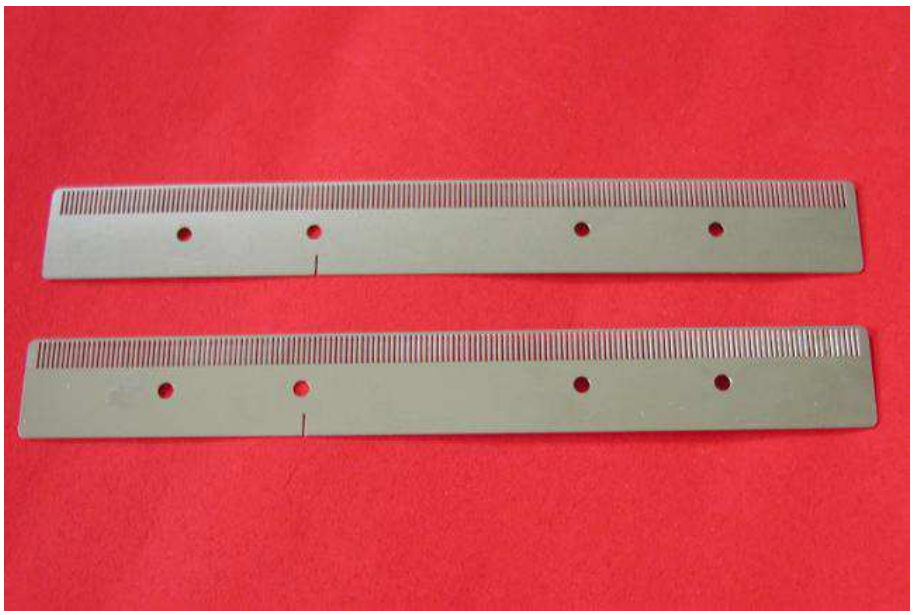

Figure 26: Two optical vanes. One side has 157 apertures to provide a quadrature signal. The other has a single slot to give a fixed reference point.

A diagram of the vane is shown in figure 26. The vane is a double-sided graticule manufactured from 0.2 mm thick steel, having 157 slots 0.3 mm wide and 3 mm long on one side of a 6 mm wide spine. The whole vane is 93.9 mm long. The spacing between slots is also 0.3 mm. There is a single similar aperture two-thirds of the way down the vane on the other side. To protect the fine features of the vane, it has a continuous edge. The vane was produced by photographic etching, and is attached to the shaft by four M1.6 fasteners. In order to ensure that the readout system provides reliable position information, the manufacturing tolerances of the apertures were kept to less than 5% of the 150 μm resolution, and the tracking error along the length of the vane was also less than this percentage. The vane and fixings have a mass of about 1 g, which is balanced about the axis of the shaft.

5.2 Laser source

Three fibre-coupled solid-state Lasers provide the light beams which intercept the vane. Commerical red (635 nm) Lasers, with a variable 0 to 2.5 mW output power are used. Visible light has advantages both for alignment and safety. The milli-Watt power level is required due to significant losses in the optical system, due to the number of interfaces such as at fibre connections. Maximising the light on the optical sensors (Section 5.5) increases the signal to noise ratio and simplifies the design of the electronic amplifiers.

In practice, the Lasers are not operated at maximum power, but at about 1 mW. This leaves sufficient overhead (both in light source and amplification gain) to adjust for any degradation in the optical fibres, e.g. due to increased attenuation as a result of radiation damage in the vicinity of the synchrotron.

5.3 Optical fibres

Two types of optical fibre are used in the light path. On the transmitting side, single mode fibres are required, in order to achieve the necessary small spot size at the collimator focal point and hence at the plane of the vane. On the receiving side, 200 μm multimode fibres are used.

The single mode fibres used are SM600 with FC/FC connectors [18]. This has a core of pure silica, which is a radiation-hard material and so ideal for the operating environment of the target. If single-mode fibres were used on the receiving side, the collimators would have to be aligned to an extremely high precision, and it would be hard to achieve an adequate light transmission. Multi-mode fibres have a higher acceptance, so make the alignment less critical. The fibres used are BFH37/200, with SMA to SMA connectors [19].

5.4 Collimators, lenses and mechanical mount

Collimators and lenses are used to focus the light from the fibres to a spot in the plane of the optical vane (where it needs to be significantly smaller than the pitch of the vane), and to

receive the transmitted light coupling it into the return fibre. The collimator is a commercial unit which produces parallel light from the diverging beam emitted by the fibre. Collimators with a focal length of 15.3 mm are used, as the longer focal length minimises the final spot size. The focusing lens, with focal length 45 mm, is attached to the front of the collimators by inserting it into a holder which is screwed onto the front of the collimator as shown in figure 27. On the transmitting side, aspheric double achromatic lenses are used to obtain the minimum spot size. On the collecting side, where focusing is less critical, double convex lenses are used to re-collimate the beam. The lenses are MgF_2 coated to minimise reflections and maximise the light transmitted into the fibres.

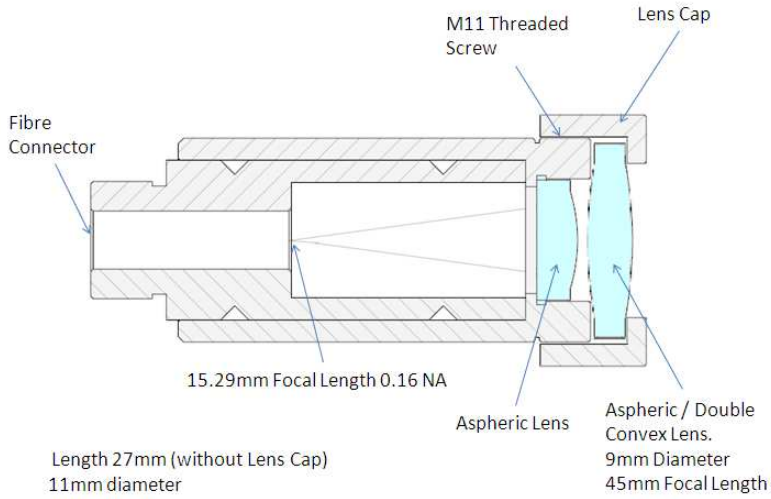

Figure 27: Cross section through a collimator and lens cap.

The optical vane moves inside the accelerator vacuum system, while all optical elements are kept outside the vacuum chamber to allow alignment adjustments. A mechanical mount was produced which has two circular sapphire windows, to allow entry and exit of the light, and provides a rigid assembly to support the optical collimator and lens units. This is illustrated in figure 28. The flat windows are bonded into metal flanges, and are rated for use in UHV environments. The pair of collimators for each optical channel is held in an arm that wraps around the mount. The exact alignment of each collimator is performed by adjusting pairs of opposed grub screws, with 4 pairs per collimator: horizontal and vertical at front and back of each collimator. The "Channel A" and "Index" arms are also adjustable in the vertical direction to allow the correct quadrature phase to be obtained and an appropriate index position to be set. The mount has proved to be easy to set up and extremely robust. Once aligned on the bench, no further optical adjustments have been necessary during periods of operation lasting several years.

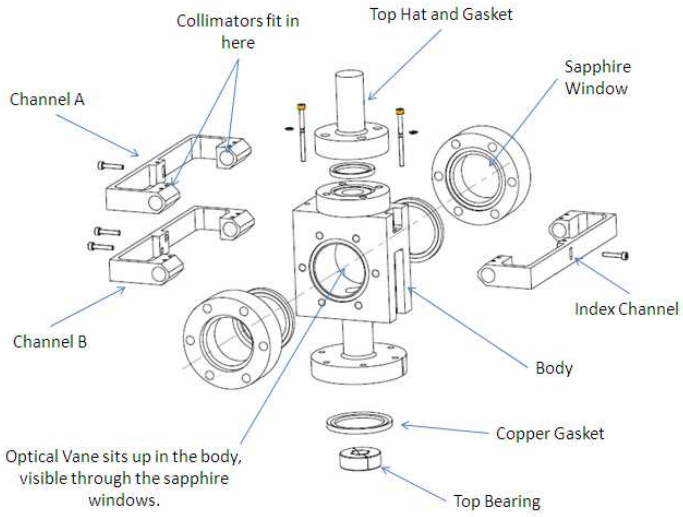

Figure 28: An exploded view of the optical mount. The optical vane sits inside the main body, where the collimators and lenses are able to focus the light.

5.5 Optical sensors

The multimode fibres are returned to a SMA photodiode (H3R880IR) [20]. This is a broad spectrum photodiode (400 to 1100 nm). As the maximum velocity of the target is less than $10\,\mathrm{m\,s^{-1}}$, the maximum data rate per channel is only 33 kHz, well within the response capability of these devices. The outputs from the photodiodes are amplified and conditioned before being converted into digital signals.

6 Stator operation and power electronics

6.1 Introduction

The target stator is a three phase brushless permanent magnet linear DC motor. Before considering how the force on the magnetic assembly changes with respect to its position within a powered stator it is necessary to understand how the coils in the stator are wired and how they are switched.

The 24 coils in the stator are split into three phases A, B and C, with eight coils in each phase. Starting from the top of the coil stack the coils are lettered in a cyclic sequence that follows the pattern, $A\ B'\ C\ A'\ B\ C'$. A block of six coils labelled thus is called a 'bank'. This sequence is repeated four times so there are four 'banks' of coils in the target stator, as shown in figure 29. All the A and A' coils are wired together in series, as are the B and B' coils and the C and C' coils. The unprimed and primed coils are wired such that when a current passes

through either an A, B or C coil in a clockwise direction then the same current passes through an A', B' or C' coil in an anticlockwise direction. The induced magnetic field direction for a primed coil is therefore opposite to that of an unprimed coil. There are two connections for each phase, one at the top of the stack and one at the bottom. The three separate connections at the bottom of the stack are wired together to form the 'star-point', while the three at the top are connected to the stator power supply, as shown if figure 30. If current is fed into one of the phases then it must return through one (or both) of the other phases. Therefore when current flows, at a minimum two phases must have current passing through them.

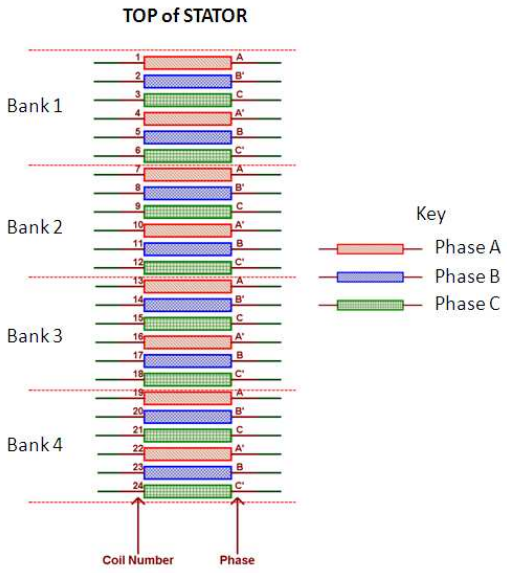

Figure 29: The relationship of phase of the coils to their physical position within the stator. Coils marked with a prime are wired so that current flows through them in the opposite direction to those that are unprimed.

6.2 Coil current switching sequence

For the target mechanism, only two of three phases are ever powered at the same time, i.e. one phase is switched to provide the current source and another phase provides the current return path. With three phases, current can therefore be switched through the stator in six different ways. Using the external connection labels A, B' and C as shown in figure 30, these six states are; $A \rightarrow B'$, $A \rightarrow C$, $B' \rightarrow A$, $B' \rightarrow C$, $C \rightarrow A$ and $C \rightarrow B'$. By stepping through these six states in a predetermined order, the coils can be switched to create a 'ripple' motion in the magnetic fields generated within the stator, as illustrated in figure 31. The direction of motion is determined by the direction in which these states are stepped through; when reversing this order the ripple motion moves in the opposite direction. By tracking the position of the magnets and correlating this position to a given state, target motion can be achieved. The required order of the states to observe this apparent motion upwards through the stator is shown in table 1.

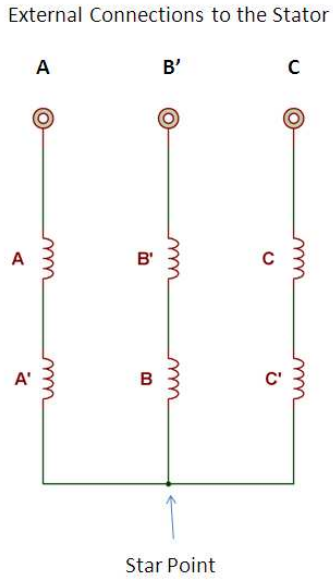

Figure 30: The wiring of the coils in the stator, illustrating the star point and the three external connections from the stator. Each coil in the diagram represents 4 coils i.e. the A coil represents the A coil from banks 1 to 4.

State	Current Flow
1	$A \rightarrow B'$
2	$A \rightarrow C$
3	$B' \rightarrow C$
4	$B' \rightarrow A$
5	$C \rightarrow A$
6	$C \rightarrow B'$

Table 1: The six states that create an apparent upward motion in the fields generated within the stator. The states are circular. Moving through the states in the opposite direction reverses the apparent motion - See figure 31.

6.3 Magnetic assembly and modelling

As described in section 3.3, the magnet assembly is composed of 3 radially magnetised rings, with a total length of 18 mm, matching the depth of 6 coils. This distance corresponds to the symmetry of the axial field, and alignment of the magnets with these fields gives the ability, with suitable feedback, to either hold the magnetic assembly in a predetermined place or to maximise the accelerating force on the permanent magnets.

A simulation of the interaction between the magnetic assembly and the coils was produced using a magnetostatic model in Opera 3D [13]. This simulates the stator in 'State 4'. (The state is arbitrary due to the symmetry of the device.) The model is axi-symmetric in R, z and the origin is placed at the centre of the stator, corresponding to a plane that sits on top of the 13th coil. For this model a current of 58 A was passed through the coils, approximately equal

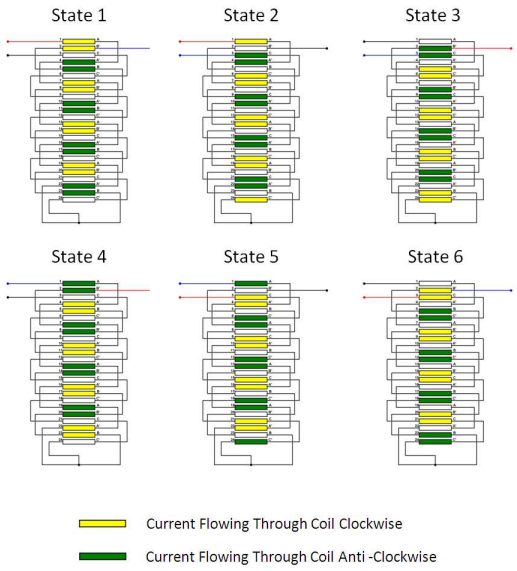

Figure 31: Switching the coils through the circular sequence given by States 1 to 6 gives an apparent motion in the coil switching upwards through the stator as illustrated. Reversing the sequence gives an apparent downwards motion. The pattern repeats itself every six coils. The permanent magnets on the target shaft can be made to interact with the fields produced by passing sequentially through these states to produce motion of the target shaft.

to the peak current during operation. The simulation ran over several iterations, and with each iteration the magnetic assembly was moved in either 0.5 mm or 1 mm increments axially along the centre line of the stator over a total distance of 20 mm. The maximum force on the magnetic assembly was calculated for each position and the results are plotted in figure 32.

Although not illustrated here the sinusoidal pattern of the force curve repeats every 18 mm, the length of one bank of coils. Figure 32 shows a clear sinusoidal pattern for the resultant force on the magnetic assembly and a sine wave can be fitted cleanly to the simulation results. Further simulations confirmed that as the magnets move towards the end of the stator bore there is no deviation from this sinusoidal pattern, as the magnet assembly is always completely contained within the stator body so end effects are minimal.

6.4 Zero-force points

From figure 32 it can be seen that there are two points for each repetition of the sine wave where the force on the magnetic assembly is zero. One of these zero-force points is unstable; movement of the magnetic assembly away from this point results in a force that pushes the magnetic assembly further away. However the other zero force point is stable, and movement of the magnets away from this zero-force point results in a restoring force; effectively this point represent the centre of a magnetic well. The stable zero-force points provide a mechanism by which it is possible to passively levitate the target shaft. The shaft will sit at an equilibrium position where the force of gravity is counteracted by the restoring force exerted by the magnetic

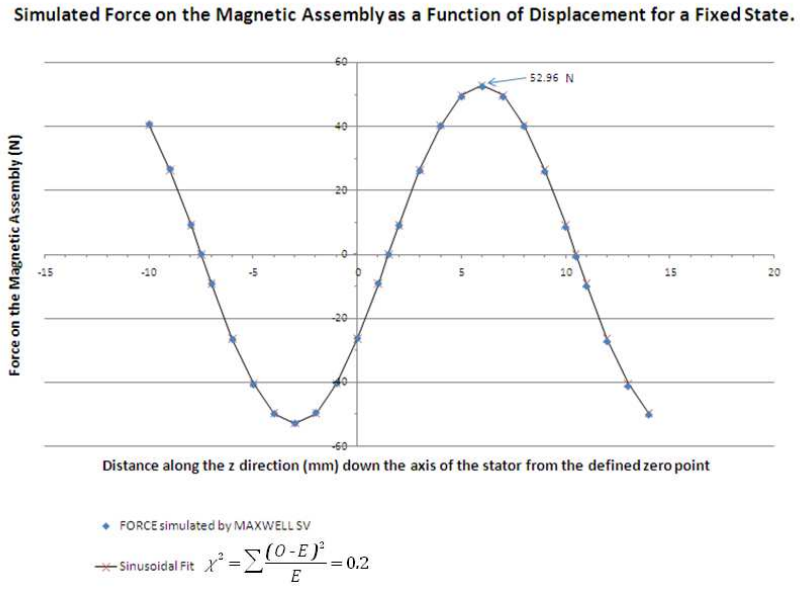

Figure 32: Simulation of the force on the magnetic assembly as a function of its position within the stator when the stator is in one of its six states with a coil current of 58 A. A good sinusoidal fit can be made to these points as illustrated.

force. Any small deviation from its equilibrium position would result in the shaft undergoing damped harmonic motion (where the damping would primarily come from the frictional forces between the shaft and the bearings). The stator is designed to be a high acceleration device, accelerating the target in excess of 80 g. Stable levitation should occur when the electromagnetic force on the shaft is equal to 1 g. To a good approximation the force scales linearly to the coil current so stable levitation of the target shaft in close proximity to these zero-force points can be achieved with a coil current that is much smaller that that required to achieve the high accelerations needed to insert the target into the ISIS beam.

The zero-force points in figure 32 are shown for the stator in 'State 4'. If the state sequence is progressed then the positions of these zero-force points move in step with the state sequence. Moving forward through the sequence moves the zero force points up through the stator in 3 mm increments, likewise moving backwards through the sequence moves the zero force point down the stator in 3 mm decrements. If the zero-force point is utilised to levitate the target shaft then the shaft will track the movement of these zero-force points as the state sequence is progressed. When the state changes the shaft will move to the new point, as a restoring force will push the shaft to the new equilibrium position. This is illustrated in figure 33. The shaft will undergo damped harmonic motion as it settles at this new point.

The ability to move and hold the shaft in this way is utilised to control the target shaft position when the target is not actuating. For example by switching the coils to the appropriate state when the target system is powered up, the target shaft is picked up from its resting position, also known as its 'parked' position, and then moved to its holding position by progressing cyclically through these states. This final state, the 'hold mode', then holds the shaft indefinitely until

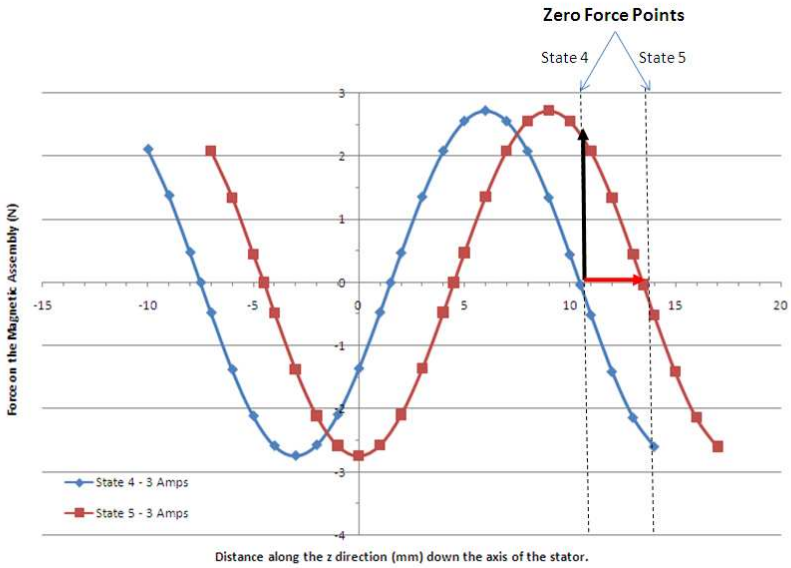

Figure 33: If the shaft was sitting at the zero-force point that corresponds to 'State 4' and the stator was switched to 'State 5' then the magnets would see a restoring force (black arrow) that would move the shaft to the new zero force position (red arrow) 3 mm further up the stator. By repeatedly incrementing or decrementing the states the shaft can be moved up and down the stator body. This graph shows the force for a 3 A coil current typical of that used to levitate the shaft.

actuation is required. Reversing the process allows the shaft to be lowered back down to its 'park-mode'.

Using the stator in this way to control the target shaft does limit the positioning of the shaft to one of a set of predefined points that are 3 mm apart. This means that the hold position is not entirely arbitrary, but the 3 mm step size gives enough freedom to ensure that the target shaft is held out of the way of the ISIS beam in 'hold-mode'. This system of moving the target shaft by allowing the magnets to track the position of the zero-force points is entirely passive and does not require any positional feedback to operate.

6.5 Actuation

From figure 32 it can be seen that the zero force point is half way between two maximum force points; we define a maximum force point as a position within the stator where the magnets on the target shaft would experience a maximal repulsive force. For each set of two maximum force points one of them will push the magnets in one direction whilst the other will push the magnets in the opposite direction. Figure 32 shows that these maximum force points are positioned ± 4.5 mm away from the zero force points; this is of course true for any zero force point in any one of the six states that the stator can be in. It can be seen that the forces change very little ± 1.5 mm either side of the peak. Integration of the fitted sine wave ± 1.5 mm either side of the peak shows that the average force is 95.5% of the peak force. If the shaft was levitated at a zero force point and the stator coil state was to either increment or decrement by two states

this would then put the shuttle magnets 1.5 mm on the far side of one of the peak forces as the zero force point would have been moved by 6 mm. At this point the shaft would accelerate back towards the shifted zero force point. In either case the resultant force would cause the shaft to pass through the location of the peak force during the first 3 mm of acceleration, as illustrated in figure 34.

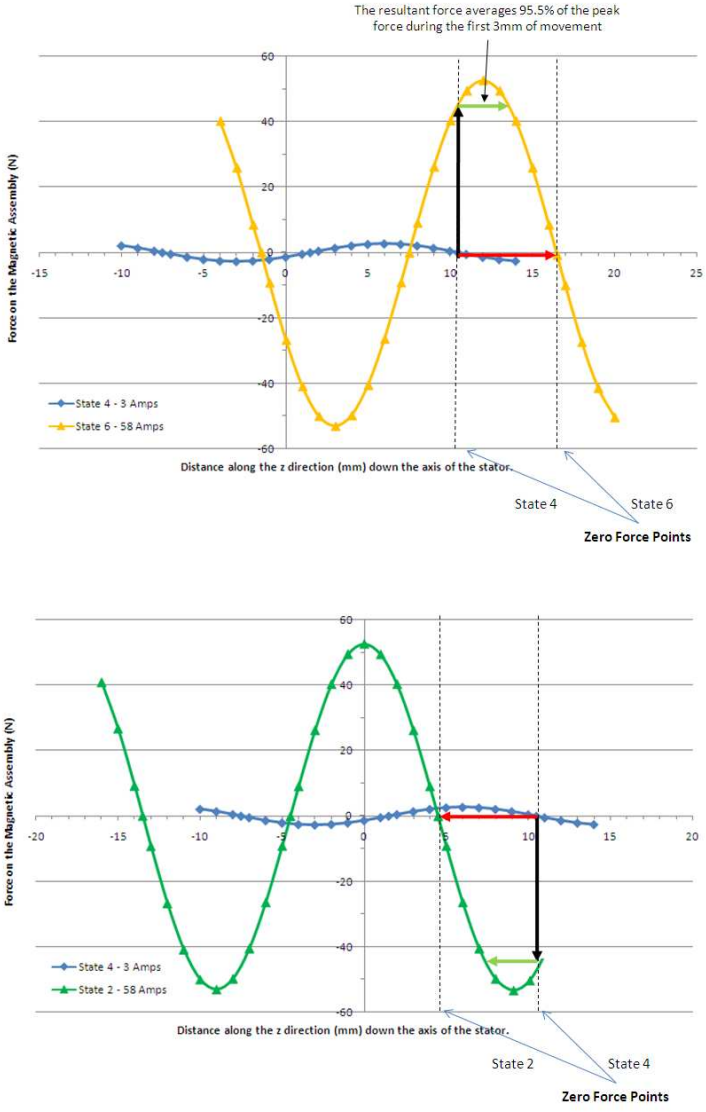

Figure 34: If the shaft was sitting at the zero-force point that corresponds to 'State 4' and the stator was switched to 'State 6'(top) or 'State 2' (bottom) then the magnets would see a restoring force (black arrow) that would move the shaft towards the new zero force position. During the first 3 mm of movement the shaft would see an average force that is ≈96% of the peak force.

If after switching the coil two states no further switching was done the shaft would continue to accelerate towards the new zero force point 6 mm further up or down the stator and would execute

damped harmonic motion about this point until it came to rest. However because the position of the shaft can be tracked using the optical quadrature system then another state change can be made when the target has travelled 3 mm, placing the magnets 1.5 mm on the far side of the next force peak. This has the effect of maintaining a maximal accelerating force on the shaft. This process can be continued down the entire length of the stator as illustrated in figure 35. If the shaft is accelerated via this mechanism, deceleration can be achieved by switching the coil state by three positions. This has the effect of placing a force of equal magnitude but opposite direction on the permanent magnets. Once again by referring to figure 32 and comparing this to figure 31 it can be seen that a switch of three states changes the direction of the accelerating force because it simply reverses the current flow through the coils. If a previously accelerated shaft is decelerated by this process then there will be a point where the shaft will change its direction of motion.

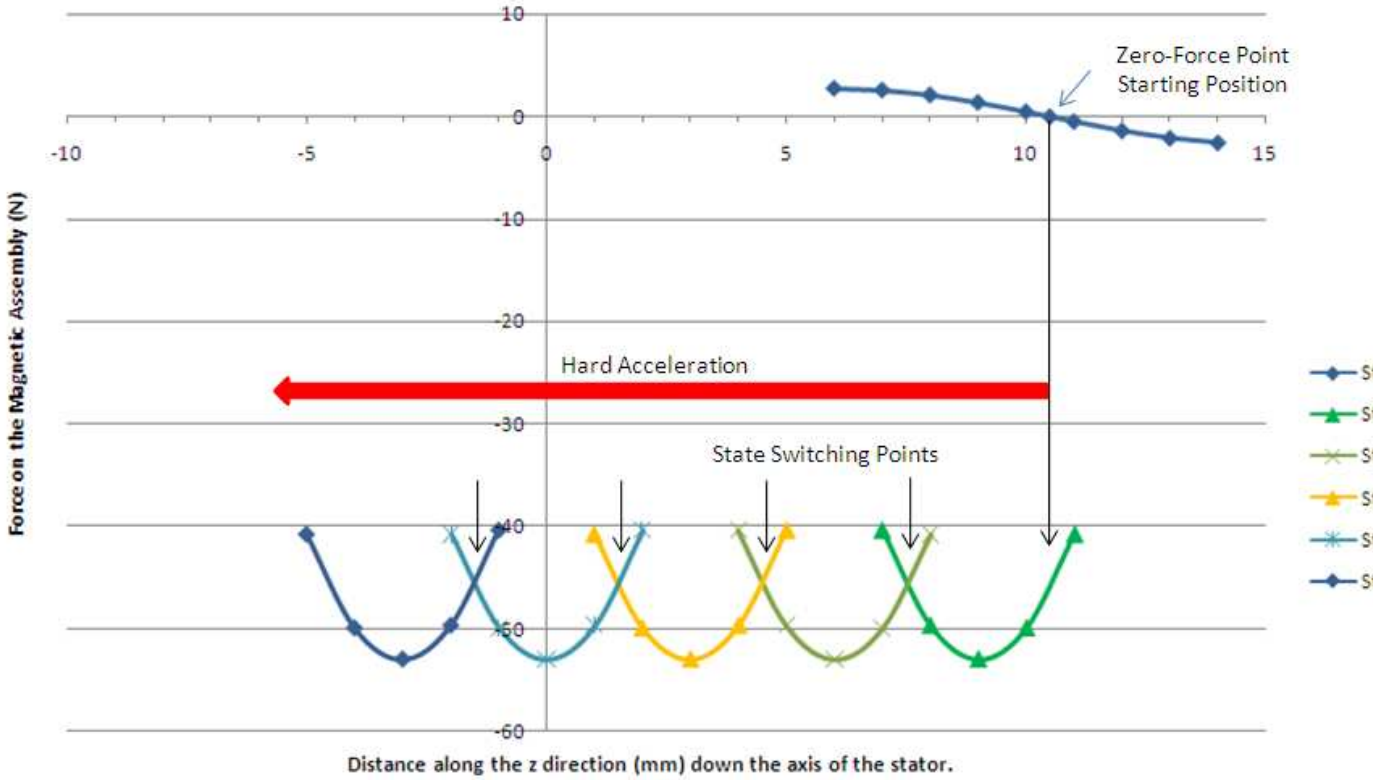

Figure 35: The shaft moves from levitation (3 A coil current) to acceleration (58 A coil current). By tracking the position of the magnets the states can be switched to ensure the shaft continually accelerates using the maximum available force. This results in a hard acceleration of the target shaft.

By monitoring the direction in which the position reading is changing, the quadrature system is able to determine the direction of motion of the shaft. This change in direction of the shaft can be used as a trigger to capture the shaft at the nearest zero-force point at the end of an

actuation. This is done by switching the stator to a state that places a zero force point close to the magnet's current position. The coil pitch of 3 mm dictates that the shaft will never be more than 1.5 mm away from a possible zero-force point and so, providing the shaft does not have a high velocity, capture of the shaft at the zero-force point is inevitable.

The processes just described provide the necessary mechanism with a suitable controller to accelerate the target into and out of the ISIS beam whilst enabling its capture again at the end of the cycle. As already alluded to, controlling the shaft's motion in such a manner is called 'actuating'. The minimum positional resolution required to control the target shaft in the way described is 1.5 mm whereas the optical system provides the shaft's position to within 150 μm. As will be described in the next section the high resolution of the optical system allows better control of the actuation depth of the trajectory of the target shaft than the minimum positional resolution requirement would allow. A full description of how the target electronics controls the trajectory of the shaft using the mechanisms just described will be discussed in a later section although figure 36 shows the principle of how it is done.

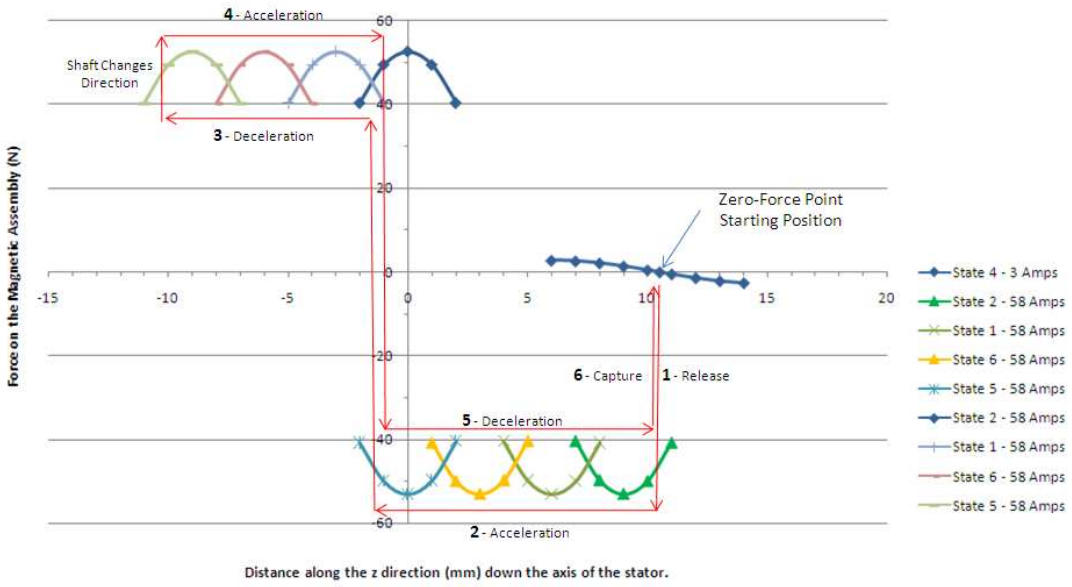

Figure 36: An actuation. The shaft is accelerated downwards, decelerated, accelerated upwards, decelerated and then captured. The position of the shaft must be tracked accurately so the controller knows into which state to put the coils to maximise the accelerating/decelerating forces.

6.6 Coil switching and current control

It has been shown that by wiring the stator in three phases and applying the appropriate currents to those phases it is possible to control the movement of the target shaft. To do this effectively there are two principal design requirements. The first of these is the ability to switch current bi-directionally through any two of the three phases, and the second is the ability to control the amount of current that passes through the coils. The rest of this section explains these

requirements in more detail and describes the power supply that provides these three controlled phase currents to the target mechanism.

Switching current bi-directionally through the three phases of the stator can be accomplished using six transistors arranged in three pairs, where each pair of transistors is connected together serially between the power rails of the power supply. The mid-point of each pair of transistors then connects to one of the three phase wires of the stator. Figure 37 illustrates how these transistors are connected. This type of circuit is known as a 'Hex Bridge' or 'Three Phase Invertor'. The three transistors across the top of the circuit are called the high side transistors as they are connected to the positive power rail, while the other three are the low side transistors.

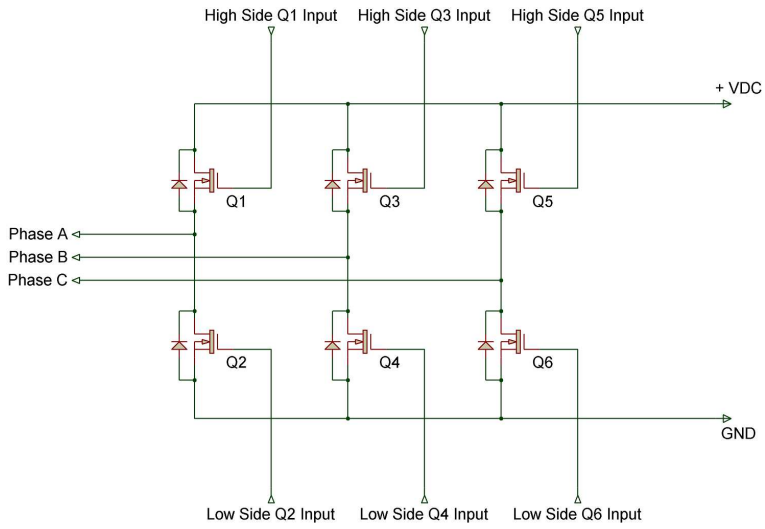

Figure 37: The Hex Bridge. This circuit allows bidirectional current control through any two of the three phases of the stator by application of appropriate control signals to the six inputs that switch the transistors on.

It is possible to see how this circuit can be utilised to switch the current bidirectionally through the phases by comparing table 2 with figure 37. The inputs are labelled in the figure Q1-Q6, often abbreviated to 1-6.

State	Current Flow	Hex Bridge Inputs
1	$A \rightarrow B'$	1 and 4
2	$A \rightarrow C$	1 and 6
3	$B' \rightarrow C$	3 and 6
4	$B' \rightarrow A$	3 and 2
5	$C \rightarrow A$	5 and 2
6	$C \rightarrow B'$	5 and 4

Table 2: How the six stator states can be switched using the Hex Bridge.

One risk that needs to be managed with this circuit is that if both transistors connected to a given phase are turned on simultaneously, e.g. if inputs Q1 and Q2 are activated simultaneously, then this creates a short circuit between the power supply rails. This will almost invariably permanently damage the transistors due to excessive current flow. This type of short circuit due to transistor switching errors is known as a 'shoot-through'. Shoot-through is also possible due to the time that it takes to switch transistors on and off. When a given transistor is sent a signal to turn it off it takes a finite amount of time for the transistor's source/drain current to reach zero. Because of this it is necessary to ensure that a certain amount of dead time is allowed before the other paired transistor can be turned on, to prevent the risk of 'shoot-through' occurring. It is worth noting that 'shoot-through' is not normally a problem when stepping through the state sequence in a circular fashion as there is always at least one state on a given phase between a low-side transistor turning off and the complementary high-side transistor being turned on (or vice versa). Given that the frequency of the state changes tends to be no more than a few kHz this ensures that the minimum dead-time is observed. However this is no longer true when the force direction is suddenly reversed. In this case both sets of transistors that are on a live phase change state and so a suitable dead time must be imposed by the controller.

When the shaft is being levitated in its holding position the gravitational force will pull the shaft slightly away from the zero-force point such that there will be a small restoring force acting upon the shaft which exactly counters gravity. The amount of counter force that the stator needs to supply to the shaft is small, reflecting the low mass of the target shaft. Ideally this equilibrium position needs to be as close to the zero force point as possible although a small offset can be accounted for. Now it can be seen from the plots that $\frac{dF}{dz}$ is maximal at the zero-force point so the amount of displacement required along the z axis to produce the restoring force is minimal and approximately linear to the applied current over short displacements.

The amount of current passing through the coils needs to be large enough that the levitation is stable but small enough that power dissipation is minimised within the stator. A current of around 3 A has been found to satisfy both of these criteria. This can be seen from figure 34; the shaft, magnets and vane has a mass of $\sim$57 g so the gravitational force is about 0.56 N. This force is counteracted by the electromagnetic force at a displacement of $\sim$500 μm from the true zero force point.

On actuation the shaft will be accelerated at $\sim 80\,g$ to intercept the ISIS beam at the correct time and to be out of the beam-pipe before the next ISIS beam injection. It has been found that a coil current of $\sim$60 A is needed to obtain the required acceleration. This current, if sustained, would quickly overheat and damage the coils and so care must be taken to ensure that the actuation current is only supplied to the stator for the required amount of time. The ability to pass a large current through the coils for short periods during actuation and to pass a smaller current through the coils for longer periods when the shaft is in its holding position means that some mechanism is required to control the current to the stator coils. By pulse width modulating the current through a given electrical component then the average current that flows through the device for a given duty cycle is, to a first approximation, linearly proportional to the maximum current that would flow through the device if the duty cycle is set to 100%.

The induction of the motor has important consequences for the driving circuit. If the design of the circuit took no consideration of the inductive currents generated by the stator then the sharp turn off of the transistors would lead to a large back emf that would inevitably destroy the transistor. Most modern power IGBTs have an internal diode across the device to protect against inductive surges.

6.7 The target power supply

Based upon extrapolation from an early 10 A prototype power supply and through simulation, it was expected that the target mechanism would require approximately 60 A of current during actuation to achieve the required acceleration. The specification, design and build for this power supply was managed by a group of electrical engineers at Daresbury Laboratory STFC. To ensure that enough overhead was built in to permit any future changes or upgrades, the power supply was originally specified to operate at up to 300 V and to provide a current of up to 100 A.

The design of such a power supply poses several problems. Having a linear power supply that could provide 100 A upon demand is possible but would be both expensive and bulky. The stator only requires the high currents for relatively short periods of time and the actual average current drawn is significantly lower than the peak current. It is therefore more economical and efficient to power the driving circuit from a capacitor bank which can provide the short high current pulses on demand when necessary. The capacitor bank is then charged by an external power supply that is designed to provide the necessary charging current to top the capacitor bank up and provide the stator's holding current. This capacitor charging unit or CCU effectively provides the average current that the stator uses, whilst the capacitor bank is there to provide the peak currents when required. The size of the capacitor bank attached to the Hex Bridge is 70 mF and is rated to 400 VDC.

The use of a capacitor bank is inherently safer than a linear power supply because should a fault occur that leaves the system in a state that demands high current then once the capacitor bank has discharged the current is limited to that provided by the CCU. The CCU used only provides a current of 4 A, and into a 3.6 Ω load (the DC resistance of two phases of the stator at 20°C) this gives a power dissipation of only ∼60 W. This is significantly lower than the power dissipation during normal stator operation when actuating at 1 Hz and so safely limits the energy deposition into the stator. At 70 mF the capacitor bank stores a significant amount of energy. This energy could be deposited into either the stator or the bridge circuit under a fault condition. Experience from the prototypes has shown that this safety mechanism is very effective at preventing the stator from overheating.

To switch the high currents necessary to drive the target power, Integrated Gate Bipolar Transistors (IGBTs) are used. These transistors switch current quickly and saturate very close to the power supply rail voltage due to a small internal resistance (R_{ON}). Both of these characteristics are good for minimising the power dissipation within the transistors and this makes them very efficient at transferring power to the load. By utilising these transistors a circuit that can switch a significant amount of power can be built with a minimum footprint. The IGBT's that were

chosen for the target power supply are power devices and can switch up to 250 A. All six sections of the gate drivers (one for each IGBT) are taken to a floating DC power supply as this gives better individual protection to the circuits.

The logic circuitry that drives the gates on the IGBT's is supplied with power from a separate power supply that is integral to the unit. The capacitor charging unit utilises a Xantrex 300-4, which can supply up to 4 A at up to 300 V, to both charge the capacitor bank and keep the stator levitated in its holding position.

Snubber circuitry has been added to the power supply to reduce the amplitude of and dampen the high frequency transients created by the pulsed switching of the transistors. This also helps to stabilise the current flow through the motor and serves to reduce EMI emitted by the motor, its power supply cable and its driving circuitry.

During development, two stator failures occurred within a period of 18 months due to electrical shorts to ground from a coil. This led to an improvement in the quality assurance procedures in selecting coils for use in a stator. Furthermore a design change of the power supply was used to reduce the effective voltage seen by the coils to ground by nearly 50%. By adding a second identical capacitor bank and a second capacitor charging unit to the system it then becomes possible to operate the stator from a split supply of -115 to $+115$ V DC. The two identical capacitor banks are charged independently but because they appear in series to the stator the effective capacitance has been halved. This effective reduction in capacitance increases the rate of discharge of the banks and so to obtain a similar actuation time the capacitor banks have to be operated at slightly above half the original voltage.

6.8 System placement in ISIS

It was clear early on in the project that the installed layout of the target system at ISIS would require considerable distances between the various components in the system. The power supply cannot be close to the target mechanism as the radiation produced by ISIS would likely cause premature failure of the electronics. It is also advantageous to have the electronics accessible so that power supply maintenance can be performed without having to wait for the synchrotron to be opened. The high currents required by the target mechanism mean that the distance to the power supply should be minimised to reduce the ohmic losses in the power cable connecting the two together. The stator coil resistances are fairly low so losses in the power cables that run from the target power supply to the target itself can be significant. For this reason the power supply to the target has been installed on the outside wall of the synchrotron at a location as close to the target area as possible. This has still necessitated a minimum power cable length of 25 m between the target mechanism and its power supply. The control electronics for the target system have been situated in the MICE control room and this is also a significant distance from both the target and the power electronics. Its installed position has meant that there is a 70 m run between the control electronics and the power electronics and nearly a 100 m run between the control electronics and the stator.

6.9 Fibre optic links

The fibre optic cables that run between the control electronics and the stator's optical block have been discussed in the section on optics. Additionally fibre optic cables are used to transmit the six signals between the controller and the power supply. The use of optical fibres guarantees signal integrity, completely isolates the power supply from the controller and eliminates the risk of noise on the signal lines which could cause additional problems with either the controller or the transistor drivers in the power supply.

This fibre optic link utilises a commercially available optical transmitter/receiver pair. The transmitter is a high powered infra-red LED with a bandwidth up to 5 MHz. This is more than sufficient as a 1% duty cycle resolution on a 20 kHz PWM signal requires a bandwidth of only 2 MHz. The receiver is a stand-alone unit that gives a TTL compatible output for use in the hex bridge driving circuitry.

The optical fibres used are the same multi-mode fibres used to return the laser light in the quadrature optical counter, (BFH37-200). These fibres are well matched optically to the transmitters, and experiments in the lab showed lower losses using these cables than using the standard polymer cables that came with the transmitter/receiver pairs. The simplicity and reliability of the optical link has meant that this optical link circuitry has remained unchanged since its initial design.

7 Target control and the data acquisition system

This section gives a description of how the target is controlled by the system electronics. The interface between the electronics and the computer that records the performance of the target, the Data Acquisition (DAQ) system, is also discussed. Figure 38 gives an overview of the major components of the target system and how they relate to each other as installed at the Rutherford Appleton Laboratory.

7.1 Target controller overview

The target controller is implemented on a Field Programmable Gate Array (FPGA), which consists of many thousands of logical units that can be programmably configured to create a bespoke digital circuit. For the target controller the logical units are configured to create a finite state machine (FSM) that both interfaces the controller to the outside world and controls the operation of the target mechanism.

The FPGA used for the target controller is a Xilinx XC3S1000 Spartan-3 FPGA. This device contains 1 million logic gates arranged as 17,280 logic cells. It has 120K of distributed RAM, 432K of block RAM, 391 I/O pins and a host of other features[1]. The FPGA has been bonded to

[1] http://www.xilinx.com/support/documentation/user_guides/ug331.pdf

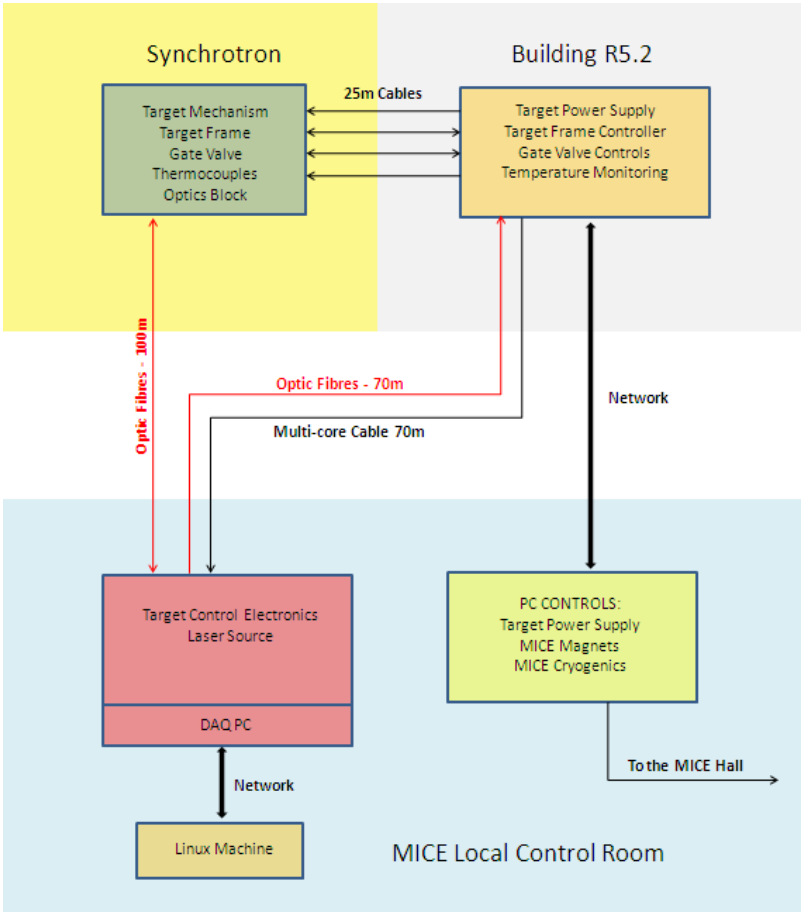

Figure 38: The major components of the target mechanism installation at ISIS, showing the relationship between the components.

a custom made PCB that permits access to most of the FPGA's IO pins and has a USB interface. The USB interface allows the FPGA to communicate bidirectionally with a PC permitting soft control of the underlying FSM based upon its current state through a GUI interface. This FPGA/PCB combination has been used in other experiments and has proven to be reliable [21].

The four states defined for the target mechanism are Parked, Hold Mode, Actuate Enable and Actuating. These are illustrated in figure 39, with the paths which connect them. The job of the FPGA controller is to control the movement of the target shaft, ensuring that it is in the correct place for its given state, the correct state being dependent upon input from both external signals and the user. The controller's FSM has many tens of sub-states to ensure that the target operates correctly in a safe manner, though this level of detail is not described here.

7.2 Control: park, hold and actuate enable modes

When the target controller and power supply systems are first powered 'on' the stator itself is left unpowered. In this state the shaft stop rests on the bottom bearing and the target is referred to as being in its 'parked' position.

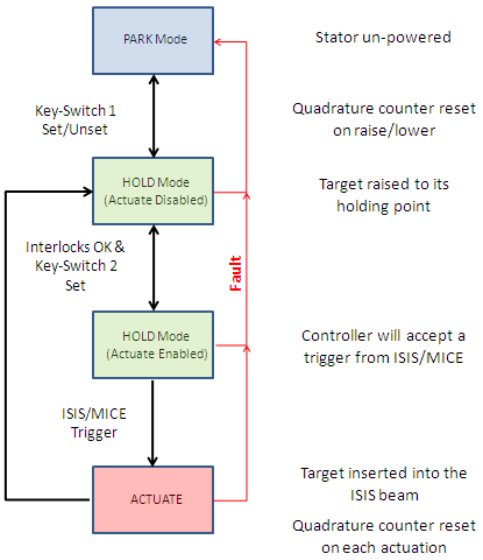

Figure 39: Diagram illustrating the four states of the target system.

Before the target can be actuated it must be moved into its 'hold' mode. This is a levitated position where the target is electromagnetically suspended at a zero-force point at a position inside the stator such that the tip of the target shaft is held outside the ISIS beam-pipe.

If the target frame was in its lowered position while the target was in park mode then this would leave the target in the path of the ISIS beam. This dictates that when the target is in its unpowered state the target frame must be in its raised position so that the target does not intercept the ISIS beam. If the target frame is put into its lowered position then the target must already be in hold mode or ISIS must be turned off. To ensure that these conditions are met the target controller will not allow the target frame to be lowered until the target is in its hold position. Conversely it will not park the target while the target frame is in its lowered position.

An enable key-switch on the front controller unlocks the system and permits it to receive control signals over the USB connection. Providing that all the interlocks are good, the controller can be commanded from the GUI to raise the target mechanism to its hold position. The latter is determined by a register value that is loaded over the USB interface and so is configurable in software. The default value is set to raise the target shaft by 51 mm, enough to hold the tip of the target out of the ISIS beam when the target frame has been lowered. The holding position is achieved by advancing the zero-force point up the stator as described in an earlier section.

Once the target has been raised to its hold position a check is performed to ensure that a correct count has been obtained by the quadrature counter and that an index signal has been received. An incorrect count or missing index signal could indicate a problem with the quadrature system and actuation would then not be possible.

The change of state from hold mode to actuate enable mode reflects a change of the internal state of the controller which is initiated by the user from the control PC. However the system

will not enter actuate enable mode until certain internal and external conditions have been met. Internally, as already pointed out, the position counter must have been reset and be reading a value that the system expects, additionally there must be no other internal errors. All the external interlocks must be good.

7.3 Control: target actuation and capture

'Actuation' refers to the state when the stator is actively accelerating the target into and out of the ISIS beam, so that it enters the beam just before extraction and is then removed from the beam-pipe before the next spill begins. Actuation is completed when the target shaft has been electromagnetically recaptured at a zero-force point. Reliable capture of the target is essential to ensure it does not fall into the ISIS beam causing the accelerator to trip off. Whilst dropping of the target shaft is unlikely to cause any damage to the target itself it could cause disruption to the operation of ISIS if it occurred frequently.

As stated in a previous subsection the controller and power supply have been designed to apply a constant force during the actuation as this gives the advantage that it is possible to control the dip depth accurately. Actuation is performed actively; the coils are switched to provide the maximum force on the permanent magnets at all times during the actuation process. For the maximum force to be maintained on the magnets the coil switching has to track the position of the target shaft and an accurate measure of the shaft's position is essential.

From a control point of view the actuation process goes through four distinct stages known as 'quadrants'. The actual capture of the target is considered a separate process in its own right. The four quadrant states are shown diagrammatically with reference to a target trajectory in figure 40.

Upon receiving a trigger signal the control system enters 'quadrant 1' of the actuate sequence. Here the controller signals the stator coils to switch so that the shaft accelerates downwards. The position of the shaft is tracked and the coils are switched to maintain the maximal force until the shaft reaches position 'switch-point 1'. This is the position at which the coil currents are reversed, and therefore determines the actuation depth. The register on the FPGA that holds the value of switch point 1 has its value calculated by the GUI, dependent upon the requested dip depth. As the resolution of the quadrature system is 150 μm this means that the target dip depth is controllable to within 300 μm (although there is a small amount of actuation-to-actuation jitter.)

As the currents are reversed the target begins decelerating and the controller enters 'quadrant 2' of the actuate sequence. The target is decelerated until it reaches a position where the motion of the target changes direction as indicated by the quadrature counter. At this point there is no physical change to the system and the coil currents are kept the same; however this change in the target direction defines the point at which the controller state moves into 'quadrant 3'. The target now accelerates upwards until it reaches the position defined by 'switch-point 2'. Here the coil currents are reversed again and the target begins decelerating; this is accompanied by the

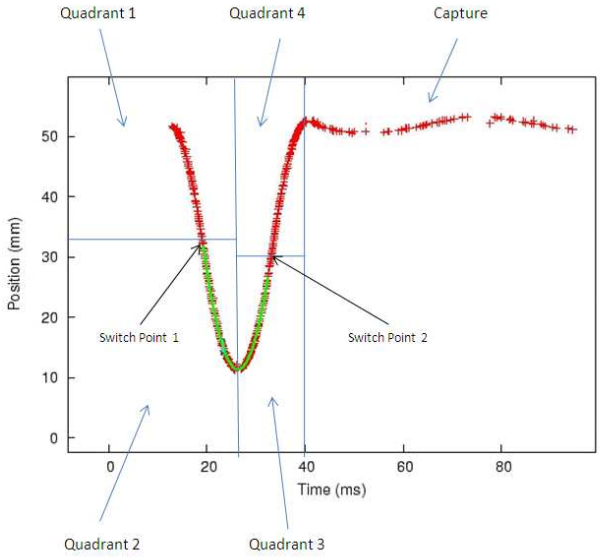

Figure 40: The actuation trajectory is split into four quadrants from the controllers point of view. Switch Point 1 reverses the coil currents and so determines the actuation depth. Switch Point 2 determines the capture point. These two points are not at the same position due to the decay on the capacitor bank.

controller state moving into 'quadrant 4'. The target continues to decelerate and at the point where the direction of the target's motion changes again the controller moves to the capture state.

When the controller enters the capture state it calculates where the nearest zero-force point is to its current position. (As described earlier, the zero force points are separated by 3 mm.) It then switches the coils to place this zero force point as close as possible to the target's current location; the target is then left to be passively captured into this zero-force point. Ideally if 'switch-point 2' is set to the correct value then the capture position should be the same as the hold position. If the zero-force point does not correspond to the target's hold position then after capture the target will be moved to the hold position ready for the next actuation.[2]

Switch-point two is offset with respect to switch-point 1 because the decay on the capacitor bank means that the rate of acceleration in quadrant one and two is greater than that in quadrants three and four. Changing the dip depth changes both the switch points by an equal amount. If the value of switch point 2 is too high or too low this results in the target being captured at either a higher or lower zero force point. If under/over capture occurs persistently then the controller will automatically make a correction to the switch-point 2 offset until the target is being captured at the hold point. This system of using 'quadrants' to define the actuation cycle allows the target to be accurately tracked by the controller as it passes through

[2] Because the shaft will have some small velocity by the time the change of direction is detected, it is necessary to reverse the current flow again for a short period of time to arrest this residual velocity. Typically this is done for a few hundred microseconds. This process is called a 'kickback' and without it reliable target capture proved not to be possible.

the trajectory ensuring reliable actuation.

7.4 The ISIS trigger signal

The triggering system for the target is fairly straightforward but has been designed with some flexibility in mind. In designing this system three assumptions were made:

1. The target must synchronise with ISIS, but the timing signal that is received from ISIS may not arrive when the target system needs to start actuating.
2. The exact time that the target intercepts the ISIS beam may need to be altered.
3. The target may also need to synchronise with another component of MICE.

Before considering these assumptions it is useful to consider some of the timing implications for running the target system.

The whole target actuation sequence for a a 44 mm strike takes about 30 ms so it takes about $14 - 15$ ms to get from the hold point to the apex of the actuate trajectory. The actual timing is dependent upon the actuation depth, and the target accelerates harder when moving into the beam-pipe than when it is moving out of it because of capacitor bank discharge ($\sim$10% reduction in current during actuation) and gravity ($\sim \pm 1\%$ each way).

The ISIS beam is injected into the synchrotron just 10 ms before it is extracted, so the target system needs to start actuating before the beam is injected if it is to catch the beam during the last 2 ms of its time in the synchrotron. The ISIS triggering system has some flexibility and can provide a timing signal from $\sim$5 ms before injection up to extraction, but this earliest time is not sufficient to allow triggering from a given ISIS injection signal (ISIS MS) to intercept that same spill before extraction.

The timing of the target actuation also needs tuning to optimise the particle production for MICE. This is firstly because the target trajectory is dependent on the actuation depth. The deeper the target has to actuate, the earlier it must be triggered as it takes longer to reach the apex of its trajectory. Secondly the timing of the interception point of the target with the ISIS beam must be adjustable. The acceleration of the target during actuation is effectively fixed so to enable an adjustable interception of the ISIS beam requires some mechanism to control exactly when the target enters actuation mode with respect to the injection of the ISIS beam into the synchrotron.

Both of these problems are solved by the use of programmable delays. To allow synchronisation of the target with ISIS so that insertion occurs in the last 2 ms of a given ISIS pulse it is necessary to use the ISIS MS signal from one spill to trigger the target to be inserted into a later ISIS spill. The ISIS control room wishes to monitor the beam loss produced by the target and they have a system that monitors this loss on the specific spills that coincide with the trigger signal

sent to the target. If the beam loss regularly exceeds a given limit on such spills then ISIS will be stopped. Because of this setup the target cannot be inserted into the next ISIS pulse after receiving the trigger but must wait for a further 2^n spills before being inserted into the beam. (n is determined by agreement with ISIS; typically $n = 8$.) This means introducing a programmable delay of $2^n \times 20\,\text{ms} - 15\,\text{ms}$. The value of 15 ms is not critical, as a second delay is triggered from the output of the first and the output of this second delay is used to determine the actual actuation start time. All of this timing is handled by the FPGA; the only detail that the user needs to enter is the required second delay value and the mode that ISIS is running in. (ISIS can run in various modes that require different values of the first delay.)

As the target may be used in a mode where it synchronises to one ISIS pulse and actuates to intercept a later one there must be some way of communicating this to the rest of the MICE so that the experiment can be synchronised to the target operation. The target system has outputs that are used to indicate that the target is actuating but additionally it incorporates a 'target ready' output and a 'MICE OK' input allowing it to handshake with an external synchronisation system. This would prevent the target from actuating until the rest of MICE was ready. For example it will be useful for ensuring that the target only actuates when the MICE RF and the MICE DAQ are ready. Such a system has not yet been implemented but it is envisaged that it will be necessary as further components of MICE are installed [22].

7.5 DAQ

Monitoring and recording of the target position is necessary on an actuation-by-actuation basis to allow analysis of the performance of the target mechanism. This target DAQ encompasses both the hardware that is required to physically allow the target data to be recorded and the software that transfers this data from the hardware onto a PC's hard disk drive. The software also enables both online and offline analysis of the data once it has been recorded.

The DAQ hardware starts with a local PC computer, in close proximity to the target control electronics, that contains a specialised interface - a National Instruments 6254 PCI card[3] with 48 digital inputs and 32 analogue inputs. Because of driver problems under Linux the card cannot simultaneously record both digital and analogue data at a sufficiently high sample rate for the target DAQ so currently only analogue data is recorded. Most of the signals that need to be recorded are naturally analogue, but this strategy has meant that the target position has to be converted to an analogue signal by a Digital to Analogue converter (DAC) before the signal is interfaced to the card. The analogue signals recorded are target position, beam-loss from ISIS in sector 7, beam-loss from in sector 8, and total beam-loss. (The target is situated in sector 7 with sector 8 immediately downstream.)

The target controller GUI also creates a data stream of target parameters on an actuation by actuation basis. This gives the status of the controller, as well as a record of controller settings,

[3] http://sine.ni.com/nips/cds/view/p/lang/en/nid/14126

errors and other key actuation parameters. Currently the GUI data stream is independent of the data files generated by the DAQ, however there are plans to integrate these in the future.

8 Performance

Two important aspects of the performance of the target mechanism are discussed below. The first concerns the ability of the target to meet the requirements set by ISIS and MICE for particle production. The second aspect considers the lifetime of the mechanism and the techniques developed to indirectly monitor the system's health, which is crucial for reliable long term operation inside ISIS.

8.1 Particle Production and Beam Loss

To ensure the target mechanism is generating acceptable beam losses at the correct time, several diagnostic signals are sent from the ISIS main control room to the MICE control room. These include the sum of the ISIS beam loss monitors in sectors 7 and 8, the sum of all the beam loss monitors, the beam intensity and the closest vertical and horizontal beam position monitors [23].

These voltage signals are fed into a National Instruments (NI) 6254 PCI card which samples the signals at 100 KS/s for 50 ms around the target actuation. The target position is also communicated to the card using a 10-bit parallel connection, and is recorded simultaneously with the voltage signals. The position is read at 200 KS/s to allow deglitching of the asynchronously sampled parallel bits. The combined signal and position data are then both displayed online for real-time feedback and written to disk for later analysis. The recording of particle data is handled by the main MICE DAQ, enabling later comparison to the target data by matching appropriate timestamps.

For optimum operation the target mechanism must maximise particle production for MICE whilst simultaneously minimising ISIS losses. The target achieves this by chasing the shrinking ISIS beam and only intercepting the beam during the final 3 ms of the ISIS acceleration cycle during which the pion production cross section is the highest. Then, to prevent losses at the next ISIS injection, 10 ms later the target tip must be completely outside the larger beam edge.

The trajectory of the mechanism during operation in ISIS is shown in figure 41. Two ISIS spills are represented by the blue beam intensity line and the first spill is the one which the target is allowed to enter. The target begins actuation just prior to the first spill and starts scraping the shrinking beam edge around 20 ms, when small losses can be seen. The target then intercepts the beam at around 22 ms and induces larger beam loss during the final 3 ms. The target finally moves out of the beam and reaches a safe distance of 58 mm before the next injection cycle at 35 ms. The position of the target is normally measured relative to the beam centre and this coordinate is referred to as Beam Centre Distance (BCD); as the target moves further from the beam this value increases.

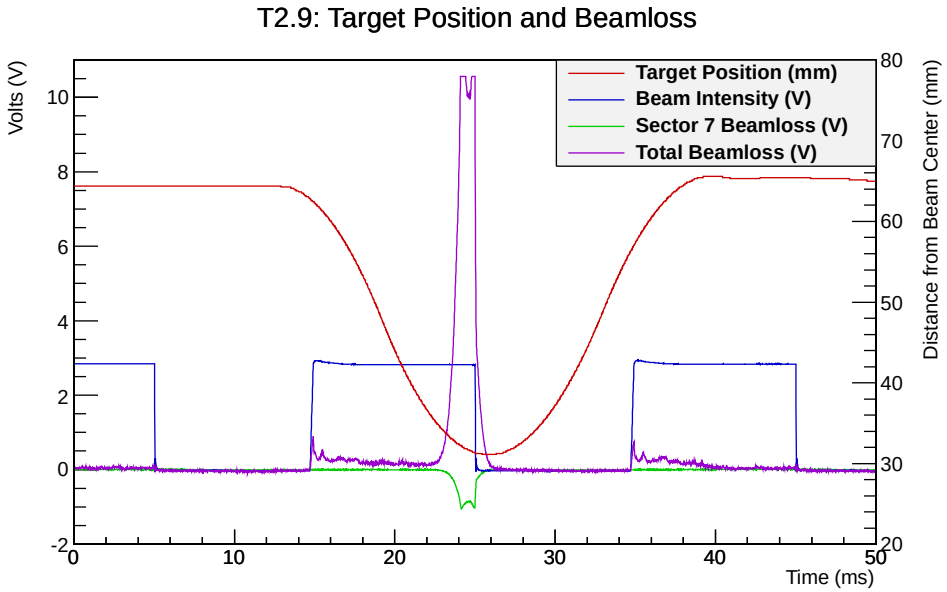

Figure 41: Signals from ISIS showing the beam intensity, total instantaneous losses and the summed instantaneous losses from sector 7, with the target trajectory overlaid. Two spills are shown by the blue beam-intensity line. The total instantaneous losses are a positive-going signal, while the individual sectors are negative-going.

The relation between the integrated beam loss over the spill in sector 7 and the particle counts per spill seen in the MICE detectors is shown in figure 42, for a 238 MeV/c μ^- beam in the MICE Step I beam-line [8]. The figure shows that for a given beam-line setting the particle rate increases linearly with beam loss seen in ISIS.

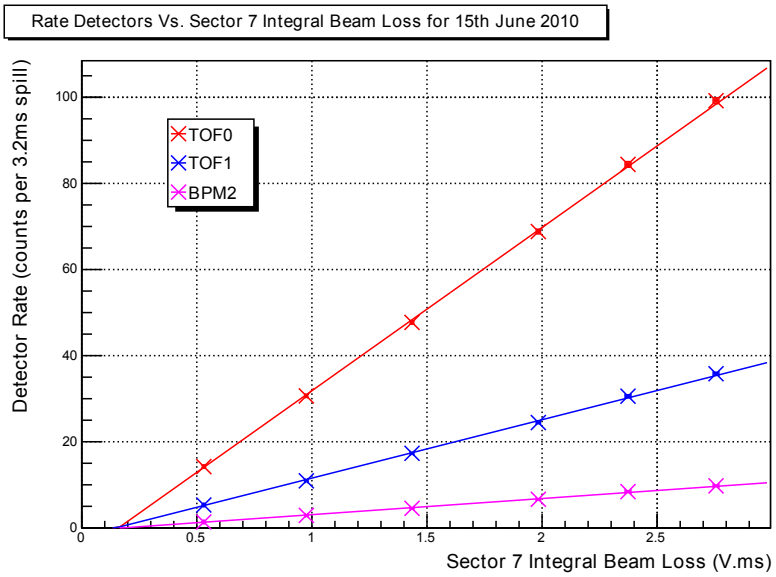

Figure 42: Particle rates in various detectors as a function of sector 7 beam loss. As the beam loss increases the particle rate for a given beam setting increases. From [24].

The effect of increasing the target dip depth is shown in figure 43, where the depth was varied from a BCD of 25 mm to 38 mm. The maximum safe depth the target can dip to is approximately 19 mm BCD. At a BCD of 25 mm the target was capable of generating between 3 and 6 V.ms of beam loss depending on ISIS conditions. Note that the target is normally limited to 2 V.ms of beam loss by ISIS [25]. The beam-loss is quite variable from run to run due to changing ISIS conditions, and the target depth is adjusted regularly to account for this.

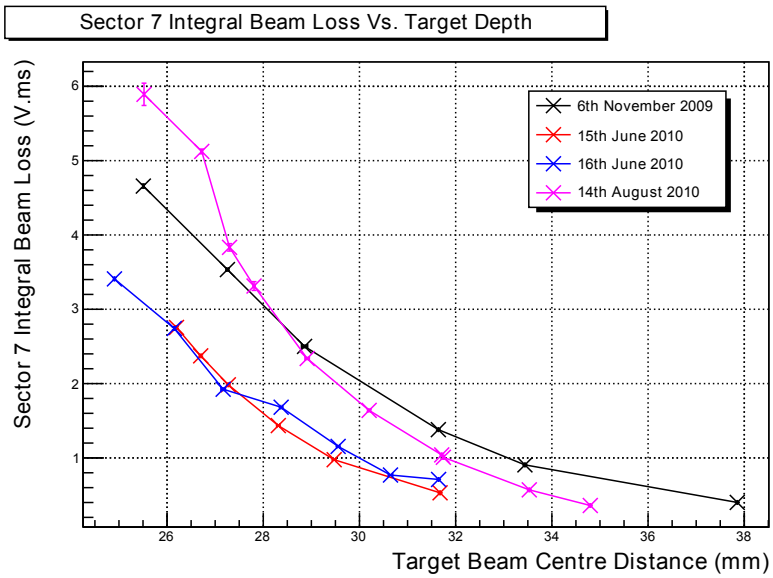

Figure 43: Beam loss as a function of target depth. While the target is capable of generating in excess of 6 V.ms of beam loss, the limits set by ISIS for regular running are normally 2 V.ms. From [24].

8.2 Target Lifetime

For operation within the ISIS vault there is a requirement that the performance and reliability of the target is well-understood. The system must be monitored to spot signs of wear and possible failure, as a damaged or malfunctioning target could disrupt the smooth running of ISIS and prevent MICE from operating.

The lifetime-limiting components of the target mechanism are the internal bearings, which limit the mechanism's life to millions of actuations. The bearings are buried deep within the stator body preventing direct visual inspection and monitoring. This makes it necessary to develop an indirect means to monitor the performance and bearing wear of the system.

8.2.1 Monitoring

Monitoring the mechanical performance of the target mechanism is performed using a list of key values returned from the controller after each actuation. This list includes data from the

actuation, such as the time to reach switch-point 1, the minimum position reached and any errors which occurred. This information is ideal for long term monitoring because it contains only key values, reducing the volume of data and the processing time. In addition since the data is calculated by the control algorithm during actuation it is much more precise and flexible than that collected by the NI card. The data is analysed offline using a simple ROOT [26] script to plot the performance change over time.

8.2.2 Bearing Performance

The bearing performance is monitored using two key parameters, which change as the bearings wear in a well-known way. The first parameter is the acceleration of the shaft, since any increase in friction will also cause a decrease in acceleration. This is calculated from the start of the actuation to the first switch-point (see figure 40), since the velocity of the shaft at this point ensures a good time-resolution. Unfortunately any change in the voltage or temperature of the coils also has an effect on the coil current and therefore on the acceleration. To help reduce these effects the capacitors are charged to a fixed voltage (115 V) and the temperature of the coils is recorded. Figure 44 shows the drop in acceleration over time as the bearings wear.

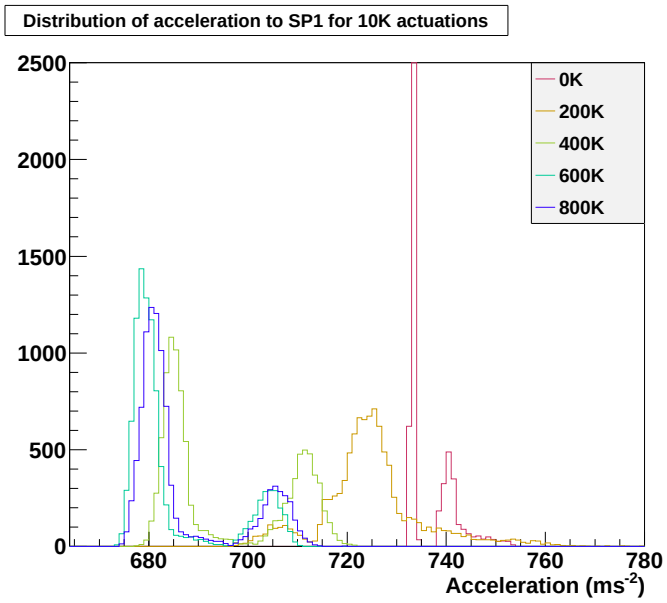

Figure 44: Acceleration for 10K actuations taken every 200K actuations for the first 800K actuations. The initial drop in acceleration caused by increasing bearing wear is apparent.

In addition to decreasing acceleration, the friction increase also allows the shaft and magnets to be captured and held further from the zero-force point at the centre of the magnetic potential (see section 6.4). This can be observed at the beginning of the next actuation when the target position is displaced from its normal starting location. This effect is monitored over time by plotting the distribution of starting positions for several hundred actuations and calculating the full width. Figure 45 shows the increase in the full width of the starting position. The increasing

jitter on the starting position also causes jitter on the minimum BCD due to the symmetry about set-point 1. An increase in jitter at the minimum BCD will increase the variability of the beam loss the target generates within ISIS and hence makes it more likely that the target exceeds the amount permitted by ISIS for that run. Note that exceeding the permitted beam loss can cause an ISIS trip and so is highly undesirable.

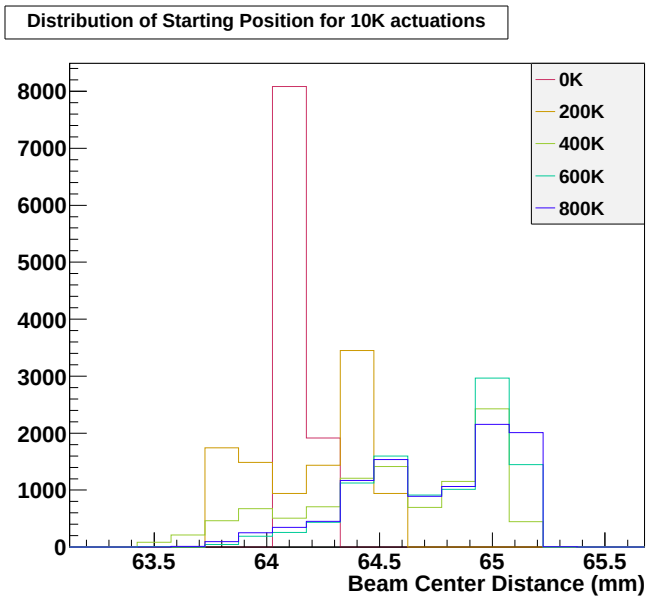

Figure 45: Starting position for 10K actuations taken every 200K actuations for the first 800K actuations. This shows the broadening as the bearings wear. The distribution increases unevenly due to a combination of effects from the magnetic fields within the stator and internal feedback used to keep the capture process stable.

8.2.3 Test Programme

To aid in understand bearing wear, develop monitoring techniques and improve bearing life an extensive test programme has been undertaken. The nomenclature used to identify the target version is Tx.y, where x corresponds to the stator number and y corresponds to the shaft/bearing combination. For testing, stator 2 was used, as stator 1 was installed inside ISIS. Each test used a freshly machined set of VESPEL bearings. For maximum wear, the maximum dip-depth (19 mm BCD) and a high dip rate (0.83 Hz) were used. For comparison, operation in ISIS typically runs at rate of 0.4 Hz and with a depth of 28 mm BCD.

Table 3 shows a summary of the bearing tests on stator 2 since the development of the FPGA-based control system. The first system tested was T2.4, which had a fully quality-assured DLC-coated shaft and a set of VESPEL bearings. The test ran for approximately 3 weeks and was disassembled at weekly intervals to check for dust. The test was terminated at 1 million actuations when the shaft begun to lock up due to wear in the anti-rotation component. This was resolved by cutting semi-circular reliefs out of the bearing as described in section 4.2.3, which was implemented in the subsequent test T2.5.

Test	Actuations (K)	Run mode	Acceptable for ISIS	Comments
T2.4	1,000	WI[a]	Y	Well polished shaft, occasional sticking during capture (outside ISIS).
T2.5	4,000	WI	Y	Weekly inspections caused a noticeable disturbance to performance.
T2.6	1,100	DS[b]	Y	Tight bearing clearances. Sticking during capture noted at end of run.
T2.7	1,300	DS	Y	Clearances re-matched to T2.5, minor increase in time before sticking during capture.
T2.8a	1,000	DS	Y	Further increase to bearing clearance, sticking began near 1 million actuations. Test paused for controller update to help alleviate sticking.
T2.8b	1,000 + 1,500	DS	Y	T2.8 test resumed with an updated controller and enabled a further 1.5 million actuations.

Table 3: Summary of bearing tests, ordered chronologically.

[a] Weekly Inspection. The target was disassembled on a weekly basis to monitor the dust produced by the bearing wear.

[b] Daily Stop. Once a day the mechanism is stopped for an hour to let the system cool and thermally contract.

The next test, T2.5 was set up identically to T2.4 and ran for over 8 weeks and 4 million actuations. Each week the bearings were inspected for dust and a small but noticeable amount was noted to build up over time (see figure 46). In the monitoring of acceleration and starting position a performance increase was noticed after the disturbance caused by each inspection. Such disturbance is not possible in ISIS and the weekly inspections were abandoned for future running.

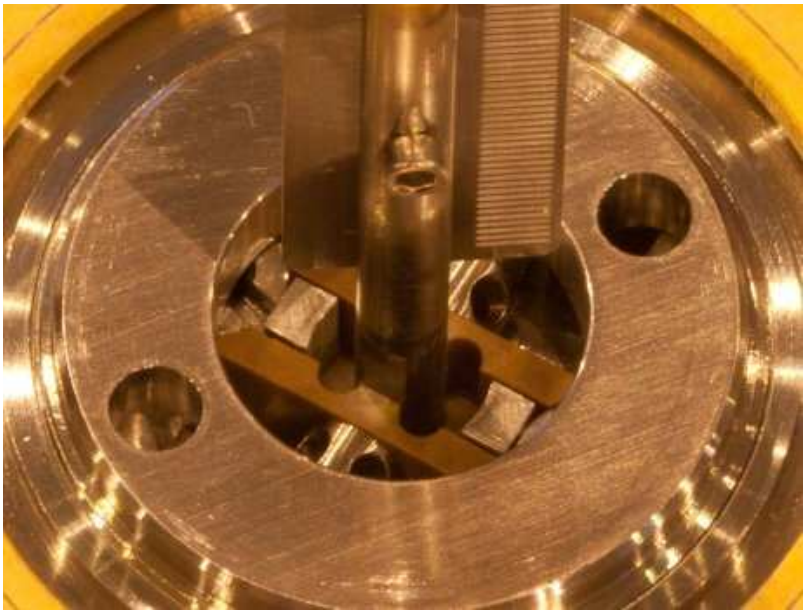

Figure 46: Image of the upper bearing of T2.4 during the final inspection after 4 million actuations. A small but noticeable amount of dust can be seen on the bearing.

The tests of T2.6, T2.7 and T2.8 all ran without intervention and with a 1 hour daily stop in place to allow the target to cool and more closely mimic ISIS operation. Each test had slightly different bearing clearances, but all exhibited similar performance. The full width of the starting position is shown in figure 47, which can be seen to broaden steadily over time with T2.7 broadening slowest. All the tests ran reliably up to 1 million actuations, but after this the target shaft began to be caught outside the defined limits. The controller is normally able to apply a low force correction to move the target into the correct location before beginning the next actuation. However, the increased friction in the bearings caused the shaft to become stuck in this state, so an improved control algorithm was put in place for T2.8b. As the update was merely for the controller, the target was not disturbed during the upgrade procedure and testing was resumed after the update. The improved algorithm was more forceful during capture and allowed T2.8 to perform a further 1.5 million actuations without inspection, bringing the total to 2.5 million actuations.

In the final inspection of the tests T2.4 through to T2.8 there was very little dust observable inside the drive, demonstrating the suitability of VESPEL bearings for use inside ISIS. This enabled the DLC on VESPEL design to be approved for use in ISIS and T2.9 was used to replace T1.0, the previous ISIS target.

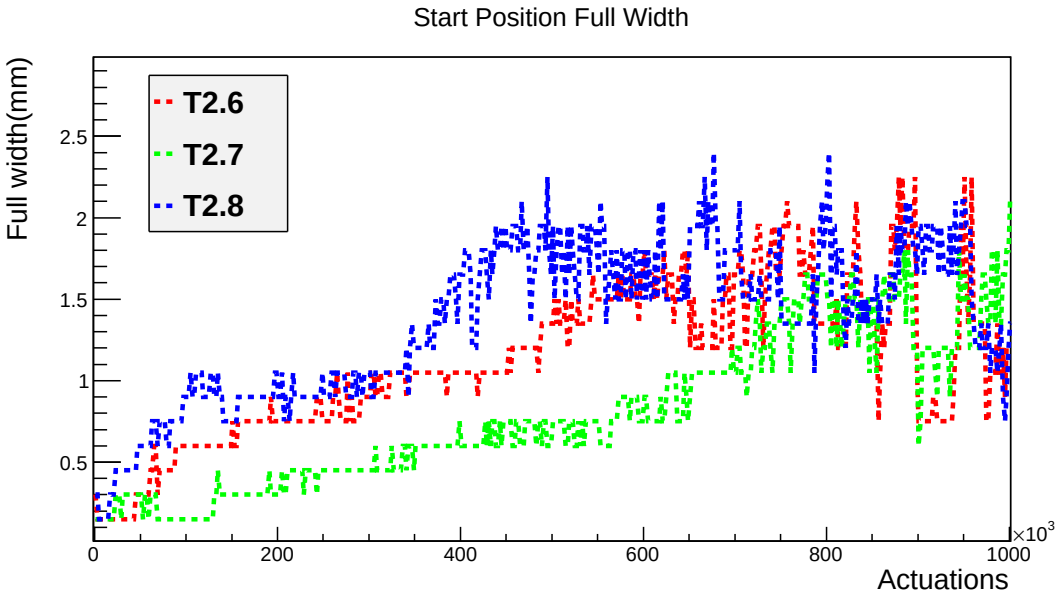

Figure 47: Width of starting position over first 1M actuations for T2.6,7,8. Capture corrections (see text) started occurring between 0.9 and 1.0 million actuations.

9 Summary

A mechanism has been presented which accurately inserts a small target into the halo of the ISIS proton beam, in order to generate particles for the Muon Ionisation Cooling Experiment. The heart of the device is a linear motor consisting of an array of radial permanent magnets inside a water-cooled bank of flat coils. The magnets are mounted on a titanium shaft, the tip of which forms the target. With appropriate remote position sensing and control of currents through the coils, accelerations of over $780\,\mathrm{m\,s^{-2}}$ are achieved during actuations, while the target remains magnetically levitated between insertions. Isolation mechanisms are implemented so that, in the case of a fault, the drive can be separated from the synchrotron both mechanically and from its vacuum system.

The most challenging part of the design has proved to be the sliding bearings which constrain the motion of the shaft. The solution adopted utilises a diamond-like carbon coating on the shaft engaging with polyimide inserts. The target drive has been tested both outside and inside the synchrotron, and detailed performance data recorded. Reliable operation has been demonstrated for several millions of actuations. Beam loss caused by the target has been monitored, and the particles produced have enabled the operation of the MICE experiment.

Acknowledgements

We gratefully acknowledge the ISIS Division at the STFC Rutherford Appleton Laboratory for the warm spirit of collaboration and for providing access to laboratory space, facilities,

and invaluable support. We are indebted to the MICE collaboration, which has provided the motivation for, and the context in which, the work reported here was carried out. We thank Dr N Schofield of the School of Electrical and Electronic Engineering, University of Manchester (and formerly of University of Sheffield) for his design of the original linear motor. We would like to acknowledge *any contractors, manufacturers, or suppliers whom we would like to acknowledge.* This work was supported by the Science and Technology Facilities Council under grant numbers PP/E003214/1, PP/E000479/1, PP/E000509/1, PP/E000444/1, and through SLAs with STFC-supported laboratories.

References

[1] S. Geer, "Neutrino beams from muon storage rings: Characteristics and physics potential," *Phys. Rev.* **D57** (1998) 6989–6997, `hep-ph/9712290`.

[2] D. Neuffer, "Multi-TeV muon colliders," *AIP Conference Proceedings* **156** (1987), no. 1, 201–208.

[3] **MICE** Collaboration, G. Gregoire *et al.*, "An International Muon Ionization Cooling Experiment (MICE)," *MICE Note* **167** (2003) `http://mice.iit.edu/mnp/MICE0021.pdf`.

[4] ISIS Pulsed Neutron & Muon Source. http://www.isis.rl.ac.uk/.

[5] Rutherford Appleton Laboratory (RAL). http://www.scitech.ac.uk/About/find/RAL/introduction.aspx/.

[6] **MICE** Collaboration, "MICE Technical Reference Document - Draft Version." http://www.isis.rl.ac.uk/accelerator/mice/TR/MICE_Tech_Ref.html, 2005.

[7] eds. S. Ozaki, R. Palmer, M. Zisman, and J. Gallardo, "Feasibility Study-II of a Muon-Based Neutrino Source," *BNL-52623* (2001) `www.cap.bnl.gov/mumu/studyii/FS2-report.html`.

[8] **MICE** Collaboration, "The MICE Muon Beam on ISIS and the beam-line instrumentation of the Muon Ionization Cooling Experiment," `arXiv:1203.4089`. Submitted to JINST (2012).

[9] N. Schofield, C. Booth, and P. J. Smith, "A low mass, brushless permanent magnet linear actuator for the ISIS target accelerator," in *50th Annual Conference on Magnetism and Magnetic Materials (MMM05)*. 2005. (Paper FF-12).

[10] "P.A.R. Insulations and Wires Ltd. Technical data MAGNETEMP CA-200." http://www.par.gb.com.

[11] "P.A.R. Insulations and Wires Ltd. Technical data DOLPHON-2102." http://www.par.gb.com.

[12] L. Howlett, "Simulation of radiation levels in the MICE target magnets." MICE Note 166, 2007. http://mice.iit.edu/micenotes/public/pdf/MICE0166/MICE0166.pdf.

[13] Ansoft, "MAXWELL SV. The student version of MAXWELL 2D." http://www.ansoft.com/maxwellsv/.

[14] A. Fasso *et al.*, "FLUKA: a multi-particle transport code," 2005. CERN-2005-10, INFN/TC-05/11, SLAC-R-773.

[15] DIN 65084:1990 Aerospace; Heat treatment of wrought titanium and titanium alloys.

[16] "Specification for material selection and the cleaning of components for use in the ISIS synchrotron systems." Rutherford Appleton Laboratory note ISIS/TS/NS/04.

[17] "Vespel® SCP-5000 Polyimide isostatic shapes typical ISO properties." DuPont^{TM} data sheet.

[18] "630 nm single mode fibre." Thorlabs^{TM} data sheet http://www.thorlabs.com/Thorcat/12600/12606-s01.pdf.

[19] "0.37 NA hard polymer-clad multimode fibre." Thorlabs^{TM} data sheet http://www.thorlabs.com/Thorcat/12200/12255-s01.pdf.

[20] "H3R880IR - FDH3 housing with FDR880IR pin photodiode." Farnell data sheet http://www.farnell.com/datasheets/99561.pdf.

[21] "The SPiDeR Collaboration." https://heplnm061.pp.rl.ac.uk/display/spider/Home/.

[22] **MICE** Collaboration, J. S. Graulich, "MICE data acquisition terminology, 2006," *MICE Note* **147** (2006) `http://mice.iit.edu/micenotes/public/pdf/MICE0147//MICE0147.pdf`.

[23] S.Payne *et al.*, "Beam diagnostics at ISIS," *Proceedings of HB2008* (2008) 466.

[24] A. Dobbs, *Particle Rate and Host Accelerator Beam Loss on the MICE Experiment.* PhD thesis.

[25] **MICE** Collaboration, I. D.Adams, R. Edgecock and K.Long, "Pion measurements with the HEP Test Beam and Implications for MICE," *MICE Note* **217** (2008) `http://mice.iit.edu/micenotes/public/pdf/MICE0217/MICE0217.pdf`.

[26] R. Brun and F. Rademakers, "ROOT - An Object Oriented Data Analysis Framework," *Proceedings AIHENP'96 Workshop, Lausanne, Sep. 1996, Nucl. Inst. & Meth. in Phys. Res. A 389 (1997) 81-86. See also http://root.cern.ch/.* (1996).